



Global estimates of evapotranspiration for climate studies using multi-sensor remote sensing data: Evaluation of three process-based approaches

Raghuveer K. Vinukollu ^{a,*}, Eric F. Wood ^a, Craig R. Ferguson ^a, Joshua B. Fisher ^b

^a Department of Civil and Environmental Engineering, Princeton University, Princeton, NJ 08540, United States

^b Water & Carbon Cycles Group, NASA Jet Propulsion Lab (JPL), California Institute of Technology, Pasadena, CA 91109, United States

ARTICLE INFO

Article history:

Received 29 June 2010

Received in revised form 6 October 2010

Accepted 7 November 2010

Available online 30 December 2010

Keywords:

Evapotranspiration

Latent heat flux

Surface energy balance

SEBS

Penman–Monteith

Priestley–Taylor

Interception

Canopy evaporation

ABSTRACT

Three process based models are used to estimate terrestrial heat fluxes and evapotranspiration (ET) at the global scale: a single source energy budget model, a Penman–Monteith based approach, and a Priestley–Taylor based approach. All models adjust the surface resistances or provide ecophysiological constraints to account for changing environmental factors. Evaporation (or sublimation) over snow-covered regions is calculated consistently for all models using a modified Penman equation. Instantaneous fluxes of latent heat computed at the time of satellite overpass are linearly scaled to the equivalent daily evapotranspiration using the computed evaporative fraction and the day-time net radiation. A constant fraction (10% of daytime evaporation) is used to account for the night time evaporation. Interception losses are computed using a simple water budget model. We produce daily evapotranspiration and sensible heat flux for the global land surface at 5 km spatial resolution for the period 2003–2006. With the exception of wind and surface pressure, all model inputs and forcings are obtained from satellite remote sensing.

Satellite-based inputs and model outputs were first carefully evaluated at the site scale on a monthly-mean basis, then as a four-year mean against a climatological estimate of ET over 26 major basins, and finally in terms of a latitudinal profile on an annual basis. Intercomparison of the monthly model estimates of latent and sensible heat fluxes with 12 eddy-covariance towers across the U.S. yielded mean correlation of 0.57 and 0.54, respectively. Satellite-based meteorological datasets of 2 m temperature (0.83), humidity (0.70), incident shortwave radiation (0.64), incident longwave radiation (0.67) were found to agree well at the tower scale, while estimates of wind speed correlated poorly (0.17). Comparisons of the four year mean annual ET for 26 global river basins and global latitudinal profiles with a climatologically estimated ET resulted in a Kendall's $\tau > 0.70$. The seasonal cycle over the continents is well represented in the Hovmöller plots and the suppression of ET during major droughts in Europe, Australia and the Amazon are well picked up. This study provides the first ever moderate resolution estimates of ET on a global scale using only remote sensing based inputs and forcings, and furthermore the first ever multi-model comparison of process-based remote sensing estimates using the same inputs.

© 2010 Elsevier Inc. All rights reserved.

1. Introduction

Evaporation from land or evapotranspiration (ET) is a combined process of evaporation of liquid water from various land surfaces (including small water bodies, e.g. lakes and rivers), transpiration from the leaves of plants and sublimation of ice and snow. The process of ET serves as one of the main phases of the hydrological or water cycle. One of the distinguishing factors of ET is its role as a linchpin between the energy and water cycles. The latent heat of vaporization, which is the energy required for evaporating water, serves as the largest single heat source for the atmosphere, thus significant in weather and climate dynamics. It is to be noted here that the transfer

of latent heat, i.e. latent heat flux (LE_{flux}), is always accompanied by vapor transfer, i.e. evapotranspiration. Thus the terms latent heat flux and evapotranspiration (or evaporation) might be used interchangeably within this study.

Although the concept of “evaporation” has been known since approximately 500 B.C. (see Brutsaert, 1982 for a chronological sketch), most of the understanding of the governing factors has been achieved in the past two centuries. Dalton (1802) was the first to point out the relationship of vapor pressure deficit ($e_{sat} - e_{act}$) of the near surface air to the evaporation rate. Later, many empirical relationships were developed based on other environmental factors (Blaney & Criddle, 1950; Hargreaves, 1975; Thornthwaite, 1948; Wilm, 1944). Based on available energy considerations and turbulent flux theory, Penman (1948) developed his evaporation equation for surfaces that are not water limited. Monteith (1964) developed a modified version of the Penman equation in which biophysics was introduced through a

* Corresponding author.

E-mail address: rkvinukollu@gmail.com (R.K. Vinukollu).

surface or canopy resistance – the now well-known Penman–Monteith combination equation – that allowed for vegetation control on transpiration rates. A somewhat simpler but effective approach was later developed by Priestley and Taylor (1972) for well watered surface by introducing a unitless constant (α , with a standard value of 1.26) to the Penman equation that represented the temperature and aerodynamic terms. Field experiments (Barton, 1979; Davies & Allen, 1973; Fisher et al., 2005; Flint & Childs, 1991) showed that the value of α was empirically related to soil moisture, and that the value decreased from its standard value for water stressed surfaces (Stannard, 1993). Many subsequent studies were conducted to include the so-called stress factors (for vapor pressure deficit, temperature, soil moisture and solar radiation) in the formulation of surface conductance (Ball et al., 1987; Dickinson et al., 1998; Dolman et al., 1991; Jarvis, 1976; Sellers et al., 1986; Wright et al., 1995).

Historically, evaporation measurements to support agriculture were based on pan evaporation, which is still widely used, or large scale weighing lysimeters. The development of instrumentation for measuring scalar fluxes and vertical wind in the 1970s led to the development of the eddy-covariance technique (Baldocchi et al., 1988; Diawara et al., 1991; Leuning et al., 1982). Today, hundreds of eddy-flux towers have been set-up globally for continuous measurements of surface water and carbon fluxes, and loosely organized under the global FLUXNET initiative. Some regional networks include the AmeriFlux, AsiaFlux, EuroFlux, OzFlux and others; all of which are members of the FLUXNET international program (Baldocchi et al., 2001). Comparing the eddy-covariance tower estimates with other ET estimates (remote sensing or model) poses two challenges (Anderson et al., 2003; Reichstein et al., 2009; Twine et al., 2000): the tower measurements rarely close the energy budget resulting in non-closure on the order of 20 to 30%, and the towers sample over a limited fetch, usually on the order of 100–1000 m depending on the tower height, which limit the scale of evaluation. Twine et al. (2000) discusses adjustments that can be made regarding closure, but recognizes that their recommended approaches (adjusting the heat fluxes based on the Bowen Ratio or the residual closure) may not always be appropriate. Also, for ease of measurement and theoretical constraints, towers are usually placed in homogeneous landscapes and therefore may not be representative of remote sensing or model resolution spatial scales.

With the addition of a thermal band on LANDSAT 3 (launched in 1978) and later with enhanced resolution and thermal bands on LANDSAT 4 (1982), high resolution (30 m visible and 120 m thermal) retrievals of land classifications and surface temperatures were made possible. These observations led to the retrieval of high resolution spatial fields of ET that were used in the FIFE (First International Land Climatology Project Field Experiment) to improve land surface parameterizations in climate models (see Sellers et al., 1995) and to develop ET estimates for irrigation management, mostly based on turbulent heat flux approaches (Allen et al., 2007; Bastiaanssen et al., 1998; Norman et al., 2003; Su, 2002; Su et al., 2005). These approaches, often referred to as energy balance (EB) algorithms, are based on the temperature gradient between the surface and the overlying atmosphere to estimate the turbulent heat transfer (i.e. the sensible heat flux, H_{flux}), with the latent heat flux being calculated as a residual of the available energy ($R_{net} - G_{flux}$) and H_{flux} . Given high resolution (120 m) LANDSAT surface temperature data, and more uniform surface air temperatures, these algorithms have proven useful for irrigation management because fields with large temperature gradients ($T_{surf} - T_{air}$) indicate low ET suggesting stressed conditions.

Although LANDSAT data is valuable for estimating ET at high spatial resolutions, the limited swath leads to a compromise on the temporal resolution (~17 days). Alternatively, lower resolution (1 to 2 km) Advanced Very High Resolution Radiometer (AVHRR) observations and Geostationary (Geostationary Operational Environmental Satellites; GOES) thermal data, while available since the late 1970s,

have not been widely used for ET at large scales due to a variety of issues such as: data accessibility (GOES), lack of ancillary radiation and vegetation data, limited computer storage amongst others. Under the NASA Earth Observing System program (EOS), the sensors on the Aqua platform (specifically the MODerate resolution Infrared Spectroradiometer (MODIS), Atmospheric InfraRed Sounder (AIRS), and the Cloud and the Earth's Radiant Energy System (CERES) offer the necessary observations of solar and longwave radiation (CERES), surface (skin and air) temperatures and atmospheric humidity (AIRS), and vegetation and land surface properties such as snow cover, emissivity and albedo (MODIS) for the estimation of ET at global scales. While the resolution is too low (5 to 25 km) for many water and irrigation management applications, it appears sufficient for climate applications envisioned under the World Climate Research Programme's (WCRP) Global Energy and Water Experiment (GEWEX) Landflux initiative (LandFlux Assessment and Organization Workshop, Toulouse, France).

GEWEX has identified quantifying ET for the global land surface critical for further understanding of Earth's climate system (Jimenez et al., in press; Mueller et al., 2010). ET is an important factor in understanding the complex feedback mechanisms between the land surface and the surrounding atmosphere, and at global scales ET equals precipitation (over long time periods, i.e. few years). Approximately 62% of the precipitation over continents is evaporated and transpired on an annual scale (Shiklomanov & Sokolov, 1985). However, such terrestrial surface estimates do not adequately describe the regional-to-continental scale variability resulting as a response to land surface heterogeneity and regional climate influences. Thus there exists a need for a completely observational-driven, spatially and temporally continuous ET product. This is only possible through remote sensing satellite products and can be achieved using measurements from various sensors onboard the EOS polar orbiting satellites. Such a dataset will help researchers better understand the continental water and energy budgets – fundamental goals of NASA's Energy and Water System (NEWS) and the WCRP GEWEX program. Also, continental estimates of ET will advance our understanding of the mean state and spatial and temporal variability of this significant component of the water cycle (Fisher et al., 2008). The above are necessary in further understanding the large scale land–atmosphere interactions related to ET.

The focus of the current study is to develop and inter-compare three process based ET products over land, based on sensors on the NASA Aqua satellite platforms and augmented by AVHRR data for vegetation characterization.

The process models considered for the current study are: Surface Energy Balance System (SEBS; Su, 2002), Penman–Monteith algorithm (PM-Mu; Monteith, 1964; Mu et al., 2007; Penman, 1948), and Priestley–Taylor based approach (PT-Fi; Fisher et al., 2008; Priestley & Taylor, 1972). The swath based retrievals are produced at 5 km spatial resolution for estimates of latent heat flux at instantaneous (W/m^2) and daily (mm) time scales. It is anticipated that these data products could serve as a Fundamental Climate Data Record (FCDR) of the Global Climate Observing System (GCOS, <http://www.wmo.ch/pages/prog/gcos/Publications/gcos-129.pdf>). The uniqueness of this study is that it provides the first ever moderate resolution estimates of ET on a global scale using only remote sensing based inputs and forcings, and furthermore the first ever multi-model comparison of process-based remote sensing estimates using the same inputs.

The motivation for the current study is evoked by one of the major objectives of the WCRP's GEWEX initiative, which is to understand the effect of energy and moisture exchange and transport processes to climate feedback. The results from the current study is a step towards addressing the challenges to meet the climate goals of an ET dataset that will provide information on the mean and variability of the components of the water and energy cycle from regional to global scales at decadal time periods.

2. Methods and data sources

2.1. Models

2.1.1. Surface Energy Balance System (SEBS)

The surface energy balance partitions the available energy ($R_{net} - G_{flux}$) between the turbulent heat fluxes (LE and H):

$$LE = R_{net} - G - H \tag{1}$$

where, R_{net} is the surface net radiation, G represents the soil heat flux and storage represented as a flux when considering water surfaces, H is the turbulent sensible heat flux, and LE is the turbulent latent heat flux. Between 1990 and 2005, new energy balance based approaches were developed specific to remote sensing needs, which include the Surface Energy Balance Index (SEBI; Menenti & Choudhury, 1993), Surface Energy Balance over Land (SEBAL; Bastiaanssen et al., 1998), Atmosphere–Land Exchange Inverse (ALEXI; Anderson et al., 1997), Simplified Surface Energy Balance Index (S-SEBI; Roerink et al., 2000), Surface Energy Balance System (SEBS; Su, 2002), and Mapping EvapoTranspiration with Internalized Calibration (METRIC; Allen et al., 2007). All the above models have been applied to estimate local to regional scale estimates of ET using some combination of remote sensing data and field observations. Anderson et al. (2007) used the 2-source ALEXI evaporation model along with data from GOES and AVHRR satellite sensors to model ET at daily temporal and 10 km spatial resolution over the continental United States for the period April–October, 2002–2004.

One of the models used in the current study is the SEBS approach which has been extensively evaluated by Su et al. (2005), McCabe and Wood (2006) and Su et al. (2007) amongst others. The SEBS model constrains the surface heat flux estimates by considering dry limit ($LE_{flux}=0$; soil moisture limitation) and wet limit (potential evaporation; only limited to available energy) conditions, thus limiting the sensible heat flux estimates with an upper and lower boundaries. Unlike many surface energy balance models, SEBS avoids the tedious process of selecting hot and cold pixels by the use of the above mentioned dry- and wet limit conditions.

The roughness parameters for heat and momentum were estimated using the kB^{-1} (inverse Stanton number) models as proposed by Massman (1999) and Blumel (1999). Considering that these models perform reliably but provide different kB^{-1} estimates over different vegetation types (Su et al., 2001), we take the mean roughness length as estimated from the two models. A flowchart of the SEBS model with the various satellite inputs is provided in Fig. 1. More details on the SEBS algorithm can be found in Su (2002).

2.1.2. Penman–Monteith algorithm (PM-Mu)

Penman (1948) developed a model for estimating evaporative flux by combining both the energy-balance and mass-transfer approaches, resulting in the well known combination equation. An important goal of Penman was being able to use standard meteorological station data that did not include surface (radiative) temperature. Also, no surface resistance term was included resulting in an equation that is valid only for open water surfaces or vegetation without water limitations. Monteith (1964) proposed that this limitation be relaxed by considering that the internal leave (stomata) vapor is saturated at the leaf temperature, the leaf surface is at the vapor pressure of the surrounding air (at the standard 2 m height) and there is a resistance that controls the transfer of vapor from the leaf to the surrounding air – the leaf resistance that is integrated up to the canopy resistance. This extension to Penman, which only required an aerodynamic resistance and now required both an aerodynamic and canopy (or surface) resistances (r_a and r_s respectively) along with the available energy ($R_{net} - G_{flux}$), results in the well known Penman–Monteith equation. Analogous approaches have been developed for soil evaporation. The Penman–Monteith equation is as follows:

$$\lambda ET = \Delta(R_{net} - G_{flux}) + \frac{\rho_a C_p VPD / r_a}{\Delta + \gamma(1 + r_s / r_a)} \tag{2}$$

where, ρ_a is the density of air, C_p is the specific heat of air at constant pressure, VPD is the vapor pressure deficit; Δ is the slope of the saturate vapor pressure curve; γ is the psychrometric constant; and, r_a and r_s are the aerodynamic and surface resistance respectively.

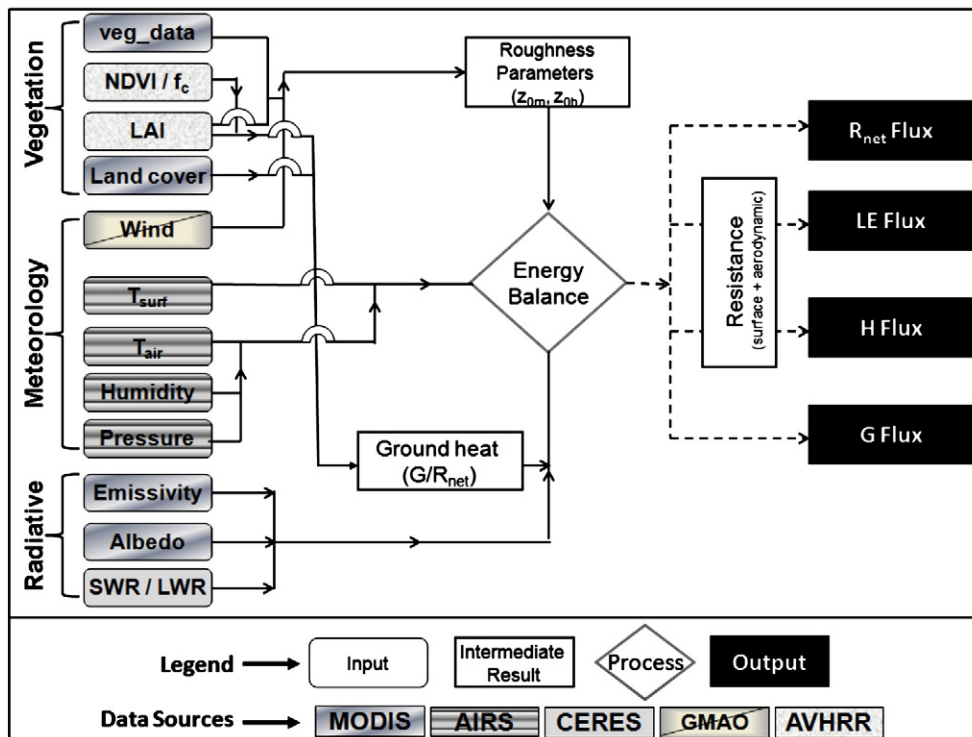


Fig. 1. Flowchart showing process involved in the surface energy balance model and the required data products and their sources.

Several studies have considered the parameterization of the surface or stomatal conductance (inverse to the resistance). For a long time the diffusion porometer was used to measure the stomatal conductance. These measurements although accurate limited the use of the variable to local scales. Later, Jarvis (1976) suggested the use of a mechanistic model in which the stomatal conductance was related to the CO₂ concentration, temperature, vapor pressure deficit and photon flux density. Similarly, Ball et al. (1987) proposed a model which parameterizes stomatal control as a function of the net carbon assimilation, CO₂ partial pressure, and atmospheric humidity. For further details on the stomatal conductance, the authors suggest Dang et al. (1997), Kawamitsu et al. (1993), Leuning (1995), Marsden et al. (1996), Oren et al. (2001), (1999), Sandford and Jarvis (1986), Schulze et al. (1994), and Xu and Baldocchi (2003).

These studies were later applied to remote sensing based models. Cleugh et al. (2007) formulated an equation for the surface conductance based on the remote sensing retrievals of normalized difference vegetation index (NDVI), leaf area index (LAI) or fraction canopy cover (*f_c*). They assumed that if there is enough soil moisture available for vegetation growth then the information is manifested in either of the above three variables on time scales that match plant growth. This formulation was further extended by Mu et al. (2007) by considering the effects of VPD and temperatures as suggested by Jarvis (1976) and others, as is described in the equations below:

$$C_s = c_L \cdot f_{T_{min}} \cdot f_{VPD} \quad (3)$$

$$C_c = C_s \cdot LAI \quad (4)$$

where, *C_s* is the stomatal conductance; *c_L* is the mean potential stomatal conductance per unit leaf area; *f_{T_{min}}* and *f_{VPD}* are the constraints by minimum air temperature and VPD to reduce the potential stomatal conductance; and *C_c* is the canopy conductance.

Mu et al. (2007) applied their resistance parameterization within the Penman–Monteith framework using MODIS-based vegetation and weather model data (the latter from NASA’s GMAO – Global Modeling and Assimilation Office) to estimate global ET at a 5 km

spatial resolution for the year 2001. For the current study, we use the Penman–Monteith model with the above mentioned resistance formulation, from now on referred to as PM-Mu, that has been applied by Ferguson et al. (2010). The only difference is that we use the same derivation for the aerodynamic resistances (*r_a*) as is used in the SEBS model. A flowchart of the model is illustrated in Fig. 2.

2.1.3. Priestley–Taylor algorithm

One the largest source of uncertainty in the Penman–Monteith equation is the parameterization of the resistances. To circumvent this problem, Priestley and Taylor (1972) developed a streamlined version, leaving only the formulation for radiation- and temperature-based equilibrium evaporation (Fisher et al, in press), and replacing all atmospheric demand with an empirical multiplier, the *α* coefficient:

$$LE = \alpha \frac{\Delta}{\Delta + \gamma} (R_{net} - G_{flux}) \quad (5)$$

where, *α* was originally set to 1.26 for well watered surfaces, thus this equation is valid for potential ET (PET) only, rather than actual ET (AET). To reduce the Priestley–Taylor PET equation to AET for remote sensing studies, Fisher et al. (2008) developed a model introducing ecophysiological constraint functions (*f*-functions, unitless multipliers, 0–1), from now on referred to as the PT-Fi model, based on atmospheric moisture (VPD and RH) and vegetation indices (normalized and soil adjusted vegetation indices, NDVI and SAVI, respectively). The driving equations in their model are:

$$LE = LE_s + LE_c + LE_i \quad (6)$$

$$LE_c = (1 - f_{wet}) f_g f_T f_M \alpha \frac{\Delta}{\Delta + \gamma} R_{nc} \quad (7)$$

$$LE_s = (f_{wet} + f_{SM}(1 - f_{wet})) \alpha \frac{\Delta}{\Delta + \gamma} (R_{ns} - G) \quad (8)$$

$$LE_i = f_{wet} \alpha \frac{\Delta}{\Delta + \gamma} R_{nc} \quad (9)$$

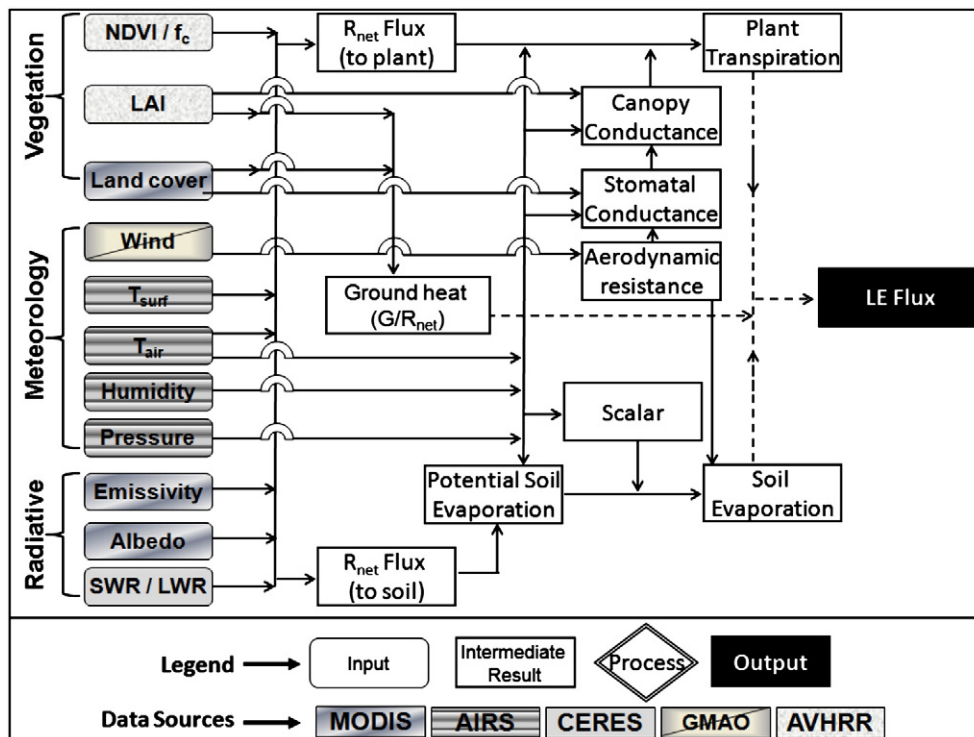


Fig. 2. Flowchart showing process involved in the Penman–Monteith based algorithm (PM-Mu) and the required data products and their sources.

where f_{wet} is relative surface wetness (RH^4), f_g is green canopy fraction (f_{APAR}/f_{IPAR}), f_T is a plant temperature constraint ($\exp(-(T_{max} - T_{opt})/T_{opt})^2$), f_M is a plant moisture constraint ($f_{APAR}/f_{APARmax}$), and f_{SM} is a soil moisture constraint (RH^{VPD}), f_{APAR} is absorbed photosynthetically active radiation (PAR), f_{IPAR} is intercepted PAR, and T_{max} is optimum air temperature, T_{opt} is T_{max} at max ($R_n T_{max} SAVI/VPD$).

Although the original PT-Fi model includes parameterization for calculating interception losses, we replace it with a uniform parameterization used across all three models (more in Section 2.1.5). Interception losses are (see Sections 2.1.5 and 2.3) subject to the scaling of instantaneous LE estimates to daily values. Fig. 3 shows the flowchart of the PT-Fi model along with the sources of the remote sensing data. More details can be found in Fisher et al., 2008. The model has been validated over 36 FLUXNET sites with an average r^2 of 0.90 and 7% bias (Fisher et al., 2008, 2009), and has been applied to large-scale studies such as the 2005 Amazon drought (Phillips et al., 2009).

2.1.4. Soil moisture dynamics

It is noted that all three models do not directly incorporate soil moisture which is an important variable when considering ET as a water budget component. Although previous studies have assumed that soil moisture availability is captured in the information provided by vegetation characteristics (like fractional vegetation cover, LAI and NDVI) and vapor pressure deficit (Cleugh et al., 2007; Fisher et al., 2008), in reality, the degree to which soil moisture controls near-surface relative humidity (and hence, VPD) varies as a function of dryness, with maximum and minimum correlation in dry (water-limited) and wet (energy-limited) regimes, respectively (Ferguson & Wood, in preparation).

2.1.5. Evaporation from snow and intercepted rainfall

The three models used in the current study are well suited for the estimation of evapotranspiration over the land surface; however, they do not consider evaporation from snow surfaces or intercepted rainfall by vegetation. Snow pack constitutes as one of the most

important aspects of water resources and hydrology in the higher latitudes (Nakai et al., 1996). Evaporation over snow covered soil and vegetation although not as high as ET from snow free regions, should be considered in monthly and annual estimates for climate studies. Evaporation from snow-covered landscapes consists of two separate components: a) evaporation from the surface (land and vegetation) and, b) evaporation from blowing snow (Bintanja, 1998; Cherkauer et al., 2003; Dery & Yau, 2001; Essery, 2001; Essery et al., 1999; Liston & Sturm, 1998; Pomeroy & Essery, 1999). Recently, Bowling et al. (2004) developed a parameterization for sublimation from blowing snow that could be applicable to remote sensing, but at this time has not been assessed fully in this context. For the current study, we ignore the evaporation from blowing snow but recognize that it needs to be included in the future work.

It has been well documented that the factors affecting evaporation process over snow are: aerodynamic resistance, wind speed, vapor-pressure deficit and radiation (Lundberg & Halldin, 2001). In the current study we assume that over a snow covered surface transpiration is negligible considering that the stomates close at freezing temperatures. With the above factors and assumptions, we calculate the evaporation over snow using the Penman equation as suggested by Calder (1990).

Interception of precipitation by dense vegetation canopies can contribute a large portion of ET. Some of the early studies (Burgly & Pomeroy, 1958; Rutter, 1967, 1968; Szeicz et al., 1969; Waggoner et al., 1969) have shown the importance of intercepted rainfall and the further process of evaporation of the intercepted water, hereafter referred to as canopy evaporation, through measurements over various biome types. However more intensive studies on interception losses have only been performed over forests. It has been reported that on an annual basis, canopy evaporation can range between 10 and 40% of the total precipitation (Rutter & Morton, 1977; Zinke, 1967), and up to 25% of the total evaporation (Shuttleworth, 1988) depending on the forest structure and cover. Rutter et al. (1971) and Gash (1979) were among the first to develop conceptual models for estimation interception losses based on canopy physiology and meteorological measurements. Later, many physically driven models

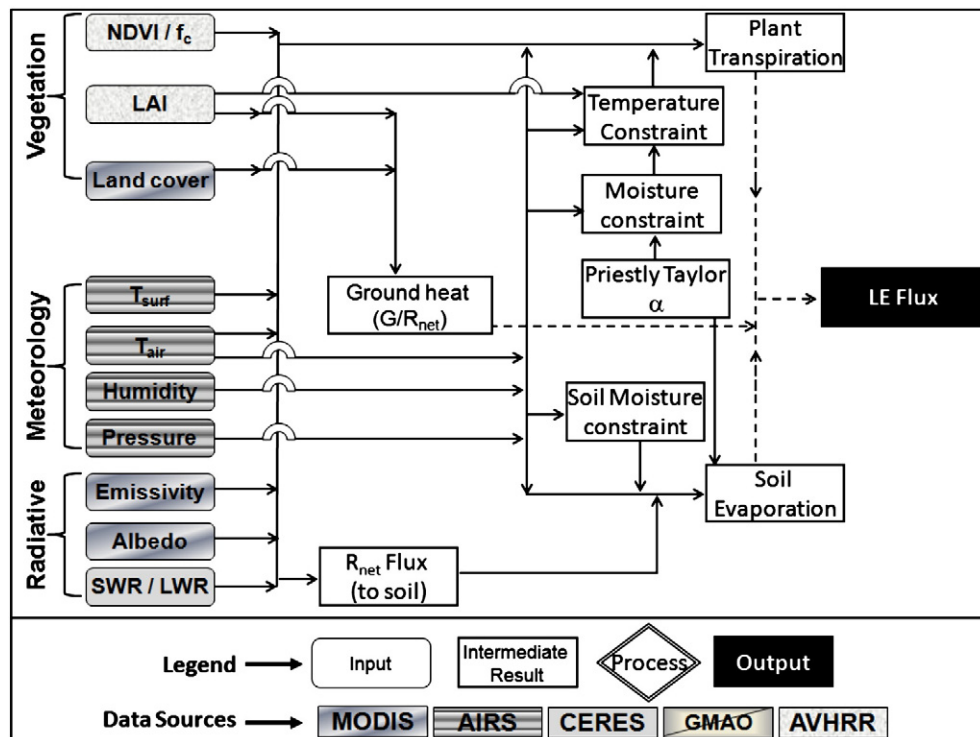


Fig. 3. Flowchart showing process involved in the Priestley–Taylor based algorithm (PT-Fi) and the required data products and their sources.

Table 1
Annual ratios (maximum) of canopy evaporation losses to the total precipitation based on land cover types.

Landcover	Interception ratio	
	Current study	Literature
Evergreen needleleaf forest	0.19	0.23 (Miralles et al., 2010) 0.17 ^a (Valente et al., 1997)
Evergreen broadleaf forest	0.15	0.14 (Miralles et al., 2010) 0.10 ^a (Valente et al., 1997)
Deciduous needleleaf forest	0.12	0.23 (Miralles et al., 2010) 0.17 ^a (Valente et al., 1997)
Deciduous broadleaf forest	0.14	0.17 (Miralles et al., 2010) 0.19 ^a (Carlyle-Moses & Price, 1999)
Mixed forest	0.19	0.13 (Jetten, 1996) 0.16 (Rutter et al., 1971)
Closed shrubland	0.1	0.27 (Navar & Bryan, 1990) 0.16–0.18
Open shrubland	0.18	(Navar et al., 1999a) 0.19 (Navar et al., 1999b)
Woody savannas	0.19	–
Savannas	0.13	–
Grasslands	0.14	–
Croplands	0.17	0.08–0.18 (van Dijk & Bruijnzeel, 2001)

^a Observed values as reported in literature.

have been developed, some of which were based on improvements of the Rutter and Gash models. For a comprehensive review of the rainfall interception models, the authors refer to Muzylo et al. (2009).

Recently, Miralles et al., 2010 developed a rainfall interception dataset based on the revised Gash's analytical model (Valente et al., 1997) model and applied globally (over forests) based on observational/satellite data from the Global Precipitation Climatology Project (GPCP) precipitation and Global Lightning Flash Rate Density dataset from NASA. Results showed that interception losses for forest covers ranged between 14 and 23% of precipitation. They indicate that the interception loss product is sensitive to rainfall intensity and the vegetation cover. Although, the above dataset can be considered as the only existing global interception data, one of the shortcomings of this dataset is that the authors assume that the canopy dries off between storm events. This assumption could lead to over estimation of the canopy evaporation especially when calculated on a monthly basis. Furthermore the data is only available monthly and over forest covers.

Considering the above limitations and practical issues, we adopt a simple mass-balance strategy based on the model suggested by Rutter et al. (1971) and further improved by Valente et al. (1997). A step by step methodology for the estimation of interception losses is presented in Appendix A. The model is applied globally on a daily basis for all vegetation covers. We use the MODIS vegetation cover (MOD12C1) with the UMD classification for distinguishing the biome types. Precipitation dataset is obtained from the Global Precipitation Climatology Project (GPCP). More details on the datasets used in the model are presented in Section 2.2. To check for reliability of the

interception product, we compare our values, based on fraction of the precipitation, to the values reported in the literature. Values obtained from the current study and literature reported values (Carlyle-Moses & Price, 1999; Jetten, 1996; Miralles et al., 2010; Navar & Bryan, 1990, 1994; Navar et al., 1999a,b; Rutter et al., 1971; Valente et al., 1997; van Dijk & Bruijnzeel, 2001) are reported in Table 1.

2.2. Datasets

The remote sensing datasets used in this study can be broadly classified into six different categories: a) Land Surface Temperature/Emissivity; b) Albedo; c) Radiation; d) Surface meteorology; e) Surface/Vegetation characteristics; and f) Other datasets. Table 2 provides an overview of the different variables, resolutions and sources. Although some variables, like air temperature, surface temperature, humidity, and radiation have a strong daily cycle, there are other variables, like leaf area index, emissivity, and albedo that do not change on a sub-daily basis. We term the former variables as Type-I forcings and the latter as Type-II forcings. For the current study, if Type-I forcings are not available, then an ET estimate is not calculated, but if the Type-II variable is missing, we substitute its climatological value based on the land cover type. The Global Land Data Assimilation System (GLDAS; Rodell et al., 2004) has mapped climatological values for land surface parameters for each land cover type using the University of Maryland (UMD) vegetation classification scheme, and this data is used here.

2.2.1. Land surface temperature/emissivity

Land surface temperature [LST; Type-I] is one of the core inputs for the SEBS model. However, it is also needed for the computation of net radiation, which is a crucial input for all the models. Considering the above importance of LST in estimating ET, one of the major considerations of the study was to use a product that is spatially and temporally consistent and having the least amount of missing data or gaps. Although, one of the finest spatial resolution LST products is available from MODIS (1 to 5 km), the quantity and quality of the data product is significantly affected by the presence of clouds (Wan et al., 2004a). Thus, for the current study we make use of the LST product from the AIRS sensor onboard NASA Aqua. The AIRS retrieval uniquely applies a cloud-clearing algorithm and provides case-by-case quality flags and error estimates. Here we use the AIRS Collection 5 Level 2 standard retrieval product (AIRX2RET) available in 6-minute granule arrays of dimension 30 (cross-track)×45 (along track) footprints. The size of these elliptical footprints range from 2.3 km×1.8 km at nadir to 7.1 km×3.0 km at the edge of the scan line (Li et al., 2008). Using only those footprint values that satisfy a quality flag of 1 (highest quality) or 2 (good quality), we produced a 0.25 gridded product (Ferguson & Wood, 2010). Specifically, an inverse-distance squared weighting is applied for all footprint

Table 2
Data variables, sources and resolutions used for generating global ET maps.

Data type	Variable	Unit	Source	Platform	Resolution
Surface meteorological data	Tair	°C	AIRS	AQUA	25 km
	Tsurf	°C	AIRS	AQUA	25 km
	Pressure	kPa	AIRS (NCEP)	AQUA	25 km
	U-Wind	m/s	CERES (GMAO)	AQUA	20 km
	V-Wind	m/s	CERES (GMAO)	AQUA	20 km
	Humidity	g/kg	AIRS	AQUA	25 km
Radiative energy flux	SWR (↓)	W/m ²	CERES	AQUA	20 km
	LWR (↓)	W/m ²	CERES	AQUA	20 km
	Emissivity	–	MODIS	AQUA	5 km
Vegetation parameters	Albedo	–	MODIS	AQUA	1 km
	LAI	–	Boston Univ.	AVHRR	8 km
	Veg. Fraction	–	Princeton Univ.	AVHRR	8 km
	NDVI	–	GIMMS	AVHRR	8 km
	Landcover (UMD)	–	MODIS	TERRA	1 km

retrievals within a 0.8 degree search radius of each cell. We note here that interpolating the 0.25 degree LST to finer resolutions, 5 km for the current study, will introduce uncertainty in the estimates because the area-averaged temperature of a pixel does not equal the temperature derived from the radiance averaged over the pixel footprint (McCabe et al., 2008a). Accordingly, all the 25 pixels (at 5 km resolution) of ET consider the same value of surface temperature as obtained at 0.25 degree resolution. The same strategy is applied for all meteorological forcings.

Emissivity, similar to the surface temperature, is utilized by all three process models for estimating the net radiation. However, not many options are available for the emissivity data product. We used the 1 km MODIS emissivity (MYD11C1) product available at 0.05 degree (~5 km) climate model grid (CMG). Considering that MODIS retrievals of narrow band emissivity are in the bands 29, 31 and 32 (Wan & Li, 1997; Wan et al., 2004b), we applied the formulation suggested by Su et al. (2007) to calculate the broadband emissivity. To account for missing data, we linearly interpolate the emissivity in time and then further perform a spatial average of the neighboring cells. As described above, emissivity can be considered as a Type-II variable and thus the GLDAS climatological values were used when the MODIS retrieval is unavailable due to cloud cover. Although the authors acknowledge that the use of emissivity and surface temperature from different sensors will result in uncertainties, there was no satisfactory quality flag available from the AIRS sensor. The surface emissivity algorithm, particularly over land, is a prime target for improvement (according to the AIRS science team) in the AIRS V6 algorithm.

2.2.2. Albedo

Surface albedo information was obtained from the MODIS MCD43B3 combined Aqua+Terra product (Jin et al., 2003; Liang et al., 2002). The albedo product consists of black-sky and white-sky albedo available at 1 km spatial and 16-day temporal resolution. To derive the overall surface albedo, we followed Su et al. (2007) by averaging the above two estimates. Alternatively, there is a CERES albedo product. However, the differences between the MODIS and CERES albedo products are as high as 10% (Rutan et al., 2009). An analysis of the CERES product (not shown) found that it lacked the expected seasonal cycle based on vegetation phenology and seen in the MODIS product. This, and the fact that MODIS albedo is available at a finer spatial resolution that better represents the land cover information, resulted in using the MODIS product.

2.2.3. Radiation

For calculating the net radiation balance at the surface, R_{net} , the following equation and data were used:

$$R_{\text{net}} = (1 - \alpha_{\text{MODIS}}) \cdot SW_{\downarrow \text{CERES}} + LW_{\downarrow \text{CERES}} - (\varepsilon_{\text{MODIS}} \cdot \sigma \cdot LST_{\text{AIRS}}^4) \quad (10)$$

where, SW_{\downarrow} is the incoming shortwave radiation, LW_{\downarrow} represents the downwelling longwave radiation, ε is the surface broadband emissivity and σ is the Stefan–Boltzmann constant ($= 5.87 \times 10^{-8} \text{ W/m}^2/\text{K}^4$). The subscripts indicate the data source of each variable. The CERES sensor is mounted both on Aqua and Terra satellite platforms and provides radiometric measurements from three broadband channels: shortwave channel (0.3–5 μm), total channel (0.3–200 μm), and the infrared window channel (8–12 μm). The Single Scanner Footprint TOA/Surface Fluxes and Clouds (SSF) product, which is produced from the cloud identification, convolution, inversion, and surface processing for CERES, is used in the current study. The cross-track mode data was preferred for our study and so data from the CERES FM3 or FM4 instruments were used accordingly. However, post March 2005 only FM3 data were used because the SW channel on the FM4 instrument failed. A complete listing of the different operation modes can be found on the CERES webpage (<http://asd-www.larc.nasa.gov/dsnyder/Aqua/>

[aqua_ops.html](#)). The data products for SW and LW radiation used were SSF-46 (Gupta et al., 2001) and SSF-47 (Gupta et al., 1992) respectively. The latest versions of the CERES SSF products that have been available only after the current study was well underway have expanded their product suite to include other variables, e.g. upward components of SW and LW radiation.

2.2.4. Surface meteorology

Surface meteorology (Type-I) information was obtained from the AIRS sensor and included surface air temperature (TSurfAir), mass mixing ratio (H2OMMRStd), and saturated mass mixing ratio (H2OMMRSat). More information on the AIRS data processing is described in the Section 2.2.2. Ferguson and Wood (2010) assessed the accuracy (bias and RMS error) of the AIRS retrievals by comparing the retrievals for surface air and skin temperatures, humidity, and model-derived surface pressure and 10 m winds from NASA GMAO to those measured at 1490 National Climatic Data Center (NCDC) surface meteorological stations over the continental US (CONUS) and Africa for 6 years (2002–2008). They found that in general, the AIRS based specific humidity (q) and air temperature (T_a) are biased dry (CONUS: -10.3% ; AFRICA: 12.4%) and warm (CONUS: $+0.2^\circ\text{C}$; AFRICA: $+1.0^\circ\text{C}$) respectively, but there is strong correlation (in some regions) between the in-situ measurements and AIRS retrievals that suggests that bias-driven errors are correctable and the data useful for ET retrievals. The current study, however, does not incorporate the suggested corrections.

2.2.5. Surface vegetation characteristics

Accurate identification of land cover type is critical for estimating ET using process scale models. MODIS based land cover type (MOD12Q1) with the UMD classification scheme was adopted for this study. The dataset is available at 1 km spatial resolution on an annual basis. Only data for the years 2003 and 2004 was available, so the 2004 land cover information was used for 2005 and 2006, assuming that there is no change. Since the product is available at 1 km spatial resolution, ET was calculated for each land cover type within a $5 \text{ km} \times 5 \text{ km}$ region and a weighted average was calculated for the final 5 km ET product. Note that the land cover information also includes the inland water surface, over which ET is estimated using the Penman equation.

Apart from the land cover information, all the three process models considered in the study make use of some combination of normalized difference vegetation index (NDVI), leaf area index (LAI), and fractional vegetation cover (f_c). NDVI information is available from the Global Inventory Monitoring and Modeling Studies (GIMMS) at NASA based on NOAA AVHRR measurements. Using these values of NDVI, the fractional vegetation f_c is computed based on the methodology proposed by Gutman and Ignatov (1998) and further improved by Zeng et al. (2000). The relationship is:

$$f_c = \frac{NDVI_i - NDVI_{\text{soil}}}{NDVI_c - NDVI_{\text{soil}}} \quad (11)$$

where $NDVI_i$ is the current value of NDVI for the grid cell. $NDVI_{\text{soil}}$ is a theoretical, intra-annual minimum value of NDVI over each land cover classification. Since for most land cover types smaller NDVI values correspond to winter values and thus have larger uncertainties due to cloud contamination and atmospheric effects than in the summer (Zeng et al., 2000), we assume a constant value for $NDVI_{\text{soil}}$ which is based on the fifth percentile for the bare soil land cover classification. $NDVI_c$ is the NDVI value for each land cover classification that corresponds to 100% vegetation cover. Based on the suggestion by Zeng et al. (2000), we estimated $NDVI_c$ using the 75th percentile for UMD land cover types 1–5 and 8–12, 90th percentile for land cover types 6, 7 and 13. The only difference in the methodology adopted for this study is that we assumed that the climatology for vegetation

changes by latitude, i.e. the maximum and minimum NDVI values for a deciduous broadleaf forest in the tropics differs from those observed at higher latitudes. Thus, the above methodology is applied based on latitude bands of 20° each, i.e. 60S–40S, 40S–20S, 20S–0, 0–20N, 20N–40N, 40N–60N and 60N–80N.

Leaf area index (LAI) is derived using the GIMMS NDVI data based on radiative transfer theory of canopy spectral invariants (Ganguly et al., 2008).

2.2.6. Other datasets

The surface pressure information is obtained from AIRS, however, the original data is an interpolated product from the National Center for Environmental Prediction (NCEP) Global Forecast System GFS 3-, 6-, and 9-hour forecasts of surface pressure. Similar to the pressure product, the horizontal wind components (u- and v vectors) are included with the CERES datasets, and are based on the analysis fields from NASA's Global Modeling and Assimilation Office (GMAO) global model. Surface wind speed is estimated by calculating the magnitude of the u- and v-vector data. The MODIS snow cover product (MYD10C1) is used at 0.05 degree Climate Modeling Grid (CMG) resolution for estimating the evaporation over snow covered regions. The product provides the percent snow cover for the pixel.

Apart from the above datasets used for estimating surface fluxes at the instantaneous (satellite overpass time) scales, a few other datasets were used for scaling the instantaneous fluxes to the daily time scale. One of the core dataset used for this is the Surface Radiation Budget (SRB; Stackhouse et al., 2000) data set. The four components of radiation (release 3.0) are available at 1° latitude–longitude with 3-hourly time steps.

To estimate a daily value of soil heat flux, we adopt the estimation procedure suggested by Bennett et al. (2008), where the soil heat flux is computed using:

$$G(t) = \frac{I}{\pi} \int_{-\infty}^t \frac{dT(0,s)}{\sqrt{t-s}} \quad (12)$$

where, I is the soil thermal inertia, $T(0,t)$ is the skin temperature (time series), s is a dummy integration variable, and t is the time. Skin temperature data for calculating daily soil heat flux was obtained from the International Satellite Cloud Climatology Project (ISCCP; Rossow & Duenas, 2004; Schiffer & Rossow, 1983). For more details regarding the processing, the authors refer to Bennett et al. (2008). Note that the skin temperature used here (daily values) is different from that used for estimating the instantaneous fluxes.

Precipitation dataset from the Global Precipitation Climatology Project (GPCP; Huffman et al., 2001) is used for estimating the interception losses. The dataset used for the current study is the Version 1.1 daily data at 1.0 decimal degree spatial resolution.

For the evaluation of the ET estimates, we used different datasets from local to regional scale. One of the first comparisons was performed using turbulent flux data from 12 eddy covariance stations obtained from the FLUXNET global network. These towers provide measurements of water and energy fluxes over 0.5–5 km² scales, and represent a wide range of biomes and climatic zones. Table 3 and Fig. 4 show the list of towers considered in this study and the corresponding biome type and climatic zone. It is to be noted that the tower selected for the current study were based upon the coverage for the 2003–2006 period with minimal missing data. Also this had to include both the level 2 (half hourly original) and level 4 (quality checked and available daily/monthly) data, and finally available to the authors as non-Fluxnet investigators.

For the evaluation at the regional scale, the authors consider calculating an inferred estimate of ET based on climatological estimates of P-Q. Section 4.3 provides more details on the above. Long term estimates of precipitation are obtained from the Global Precipitation Climatology Center (GPCC; Rudolf et al., 2003). The data is available at monthly temporal resolution at a spatial scale of 1.0 decimal degree for the period 1901–present.

Currently, there exists no remotely sensed or observation-based gridded runoff product at continuous time scales over the land surface. To incorporate the runoff term for evaluation of the water budget components, we use a climatological product that is available from the Global River Discharge Center (GRDC; Fekete et al., 2002). Two separate products were considered for the current study: an observed monthly climatology (based on in-situ streamflow measurements) over a set of selected basins and a composite global runoff field which combines observations and output from the water balance model (WBM) of Fekete et al., 2002.

2.3. Methodology

The above data are used with the three process models described earlier, to estimate the instantaneous latent heat fluxes. Following is the list of steps for the algorithms.

- i) The net radiation, R_{net} , is calculated using Eq. (10).
- ii) Soil heat flux is calculated based on the following equations.

For water surfaces (Frempong, 1983),

$$G = 0.26 \cdot R_{net} \quad (13)$$

For other land cover types,

$$G = R_{net} \cdot \left[\Gamma_{canopy} + (1 - f_c) (\Gamma_{soil} - \Gamma_{canopy}) \right] \quad (14)$$

where, Γ is the ratio of soil heat flux to the net radiation. The values of Γ for soil and canopy are 0.315 (Kustas & Daughtry, 1990) and

Table 3
Eddy covariance towers used for data comparisons in the current study.

Tower	Elev. (m)	Climate	Biome type	Lat	Lon	Closure
ARM SGP – Main (ARM)	314	Temperate continental	Croplands	36.61	–97.49	0.68
Audubon (AUD)	1469	Temperate arid	Grasslands	31.59	–110.51	0.70
Blodgett Forest (BLO)	1315	Mediterranean	Evergreen needleleaf forest	38.90	–120.63	0.55
Bondville (BON)	219	Temperate continental	Croplands	40.01	–88.29	0.56
Fort Peck (FPE)	634	Temperate	Grasslands	48.31	–105.10	0.64
Harvard (HAV)	340	Temperate	Deciduous broadleaf forest	42.54	–72.17	NA
Mead – Rainfed (MEA)	363	Temperate	Croplands	41.18	–96.44	0.85
Morgan Monroe (MMF)	275	Temperate continental	Deciduous broadleaf forest	39.32	–86.41	0.24
Niwot Ridge (NIW)	3050	Temperate	Evergreen needleleaf forest	40.03	–105.55	0.80
Sylvania Wilderness (SYL)	540	Northern continental	Mixed forests	46.24	–89.35	0.65
Tonzi (TON)	177	Mediterranean	Woody savannas	38.43	–120.97	0.42
UMBS (UMBS)	234	Temperate northern	Deciduous broadleaf forest	45.56	–84.71	NA

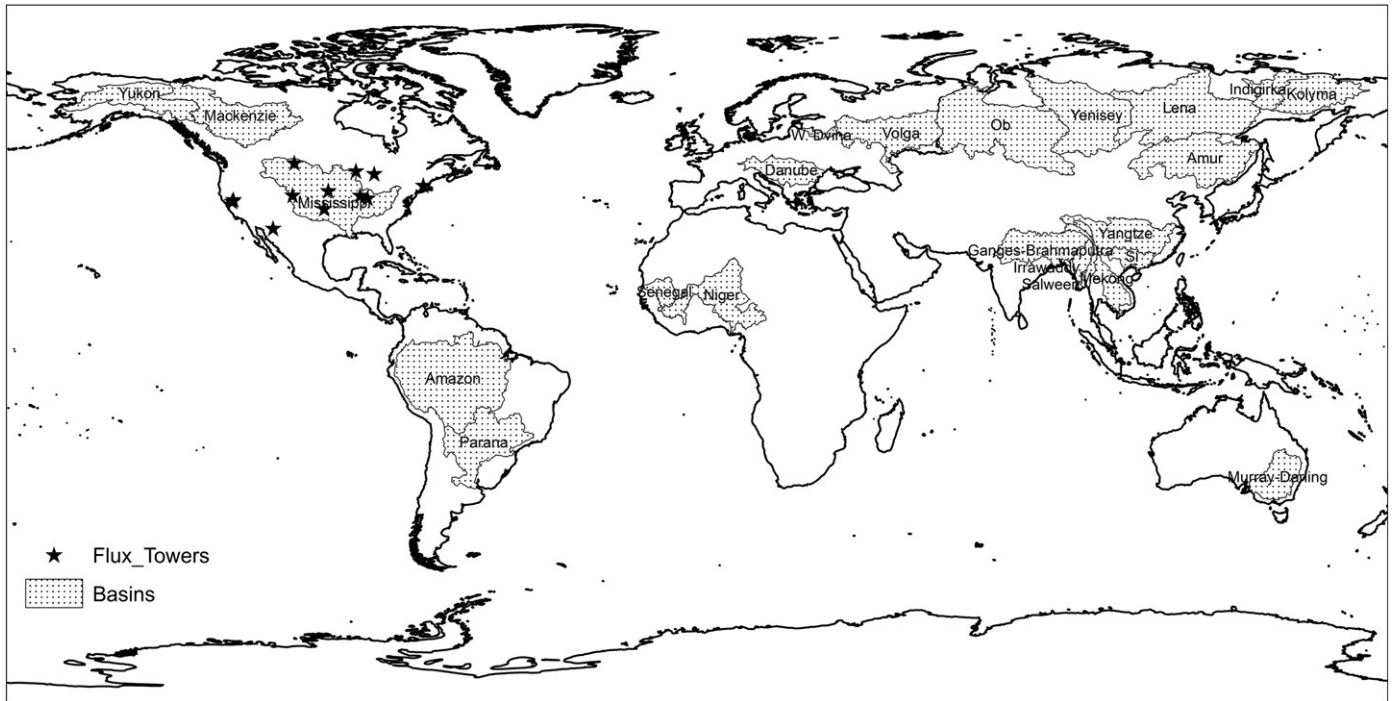


Fig. 4. Geographic location of the towers and the basins considered in the current study. Note that some of the smaller basins in northern Eurasia are plotted as part of the bigger basins.

0.05 (Monteith, 1973) respectively. For the PM-Mu and PT-Fi models, the fractional vegetation cover information is used to partition the available energy ($R_{\text{net}} - G$) between the soil and the vegetation.

$$AE_{\text{soil}} = (1 - f_c)(R_{\text{net}} - G) \quad (15)$$

$$AE_{\text{veg}} = f_c \cdot (R_{\text{net}} - G) \quad (16)$$

- iii) *SEBS model*: The roughness heights for heat and momentum are calculated.
- iv) *SEBS model*: Resistances are calculated and the sensible heat flux is calculated. Finally the latent heat flux values are estimated based on Eq. (1).
- v) *PM-Mu and PT-Fi models*: The limiting factors for vapor pressure deficit, temperature and soil moisture are calculated.
- vi) *PM-Mu model*: Canopy conductance is calculated using Eq. (4) while aerodynamic resistance is calculated using the SEBS parameterization. Latent heat flux for soil and vegetation are calculated using Eq. (2) and summed to get the final values of ET.
- vii) *PT-Fi model*: Latent heat flux for soil and vegetation are calculated using Eqs. (7) and (8) along with constraints for plant moisture, plant temperature and soil moisture.
- viii) *All models*: Latent heat flux values are estimated for snow covered regions based on the Penman equation. Based on the percent snow cover over a pixel, the latent heat flux is estimated as a fraction. However, if the surface temperature is at or below freezing, then it is assumed that there is no conductance ($= 0$) and thus no evaporation.

Daily values of evapotranspiration are needed for comparisons with other ET estimates and for further use in water and energy budget studies. Following the work of Crago and Brutsaert (1996) and Sugita and Brutsaert (1991), the instantaneous fluxes of latent heat are scaled to daily values by assuming that the evaporative fraction, obtained at the satellite overpass time, is constant throughout the day.

Using the above assumption, the daily ET value is extrapolated using the following equation:

$$ET_{\text{daily}} = \lambda \cdot n \cdot EF_{\text{inst}} \cdot (R_{\text{net}} - G)_{\text{daytime}} \quad (17)$$

where, EF_{inst} is the instantaneous value of evaporative fraction, defined as the ratio of latent heat flux to the available energy, λ is the latent heat of evaporation, and the constant n ($= 1.10$) is the factor to include night time evaporation. The daytime hours are calculated based on latitude and the day of the year. Based on the study by Sugita and Brutsaert (1991), not considering night time ET can lead to underestimation of total daily ET by approximately 7%. Although, they propose the constant to be 1.15, a smaller value ($n = 1.10$) is used in this study based on calculating the night time evaporation from the VIC land surface model and compare it to its day time evaporation. Results showed that the mean annual night time evaporation evaluated to approximately 9.57% of the day time evaporation – close to the 7% suggested by Sugita and Brutsaert (1991). The (total) daytime value of net radiation (different from the instantaneous estimates mentioned in Section 2.2.3) is obtained using the Surface Radiation Budget (SRB) dataset. The SRB dataset contains incoming and outgoing SW and LW radiation at 1.0 degree resolution and 3-hourly temporal scale. Soil heat flux at the daily time step is obtained using the ISCCP dataset, as described in Section 2.2.6.

The interception losses (as described in Section 2.1.5 and Appendix A) are added to the ET estimates, and finally we calculate a daily value of sensible heat flux (W/m^2) using the following equation:

$$H_{\text{daily}} = R_{\text{net-daily}} - G_{\text{daily}} - \lambda \cdot ET_{\text{daily}} \quad (18)$$

3. Algorithm and data evaluation

The accuracy of the ET dataset depends on two (of the many) factors: (a) The algorithms used to estimate ET and (b) the accuracy of the input datasets. Previous studies have evaluated the output from

the SEBS model. Jia et al. (2003) evaluated the SEBS model output using remote sensing inputs from Along Track Scanning Radiometer (ATSR) by comparing the sensible heat flux estimates over three different landscapes to that from a large aperture scintillometer (LAS). They found the root mean square differences in the sensible heat flux estimates of $\sim 25 \text{ W/m}^2$ (daily time scale). Su et al. (2005, 2007) evaluated the SEBS models over local- and regional scales using eddy flux tower data, MODIS and LANDSAT based remote sensing inputs and data from North American Land Data Assimilation System (NLDAS, Mitchell et al., 2004). When forcing the SEBS model with the tower based inputs, the accuracy of the model estimates ranged between 5 and 15%. However, when the model uses remote sensing and reanalysis inputs, the errors increased significantly (up to 40%), suggesting that the scale differences between the datasets affect the comparisons. Su et al. (2005) also found that the difference between the (instantaneous) remote sensing and tower based estimates can be mainly attributed to the estimation of available energy – i.e. net radiation minus soil heat flux.

The PM and PT approaches have been widely used for many years. Although, the equations are well developed, many studies have contributed to the parameterization of the surface conductance (see Section 2 for more details). Not claiming completeness, some evaluation of the approaches can be found in Allen et al. (2006), Castellvi et al. (2001), Crago (1996), Debruin and Keijman (1979), Gavilan et al. (2007), Green et al. (1984), Guo et al. (2007), Irmak et al. (2005), Lhomme (1997), Liu and Lin (2005), Ortega-Farias et al. (2004), Shuttleworth and Calder (1979), Stannard (1993), and Wang et al. (2006).

Recently, Ferguson et al. (2010) performed a sensitivity study of ET (PM-Mu estimates) based on an ensemble generation framework using different remote sensing (input) datasets. They found that although differences in the climatic variables contribute significantly

to the final ET uncertainty estimates, LAI and fractional vegetation cover have the highest impact especially in the humid basins. Su et al. (2005) using the SEBS retrieval algorithm found that the accuracy of surface fluxes and ET estimates depends on the scale and representativeness of the input datasets. Fig. 5 presents for five ET input variables (namely air temperature, mass mixing ratio, incoming shortwave radiation, incoming longwave radiation, and wind speed) scatter diagrams of remote sensing retrievals against observations from 12 eddy-flux towers. (See Table 3 and Fig. 4 for the tower locations.) We consider these are the most important variables that affect the accuracy of our ET estimates. Although, vegetation characteristics (like LAI, f_c and NDVI) play an important role in the ET estimation, continuous measurements at the tower sites are unavailable. Among the five variables, the correlations (Kendall's τ) between the remotely sensed and tower observations ranged from 0.17 to 0.83. The root mean square differences (RMSD) are also provided. It is to be noted that incoming SW and LW radiation have high RMSDs, many outliers and a consistent bias (see Fig. 5). These input differences significantly affect the correlations between the towers estimated and remote sensing estimated ET retrievals. The Level-2 Ameriflux data (<http://public.ornl.gov/ameriflux/>) were used for the instantaneous flux comparisons. Note that the above comparisons are performed using instantaneous remote sensing retrievals to the hourly observations over the towers.

4. Evaluation of the ET estimates

4.1. Local and regional scale comparisons

Fig. 6 shows the monthly mean scatter plots of R_{net} , G_{flux} , H_{flux} and LE_{flux} between tower based (hourly scale) and the remote sensing (instantaneous) estimates. Note that the tower data are available only

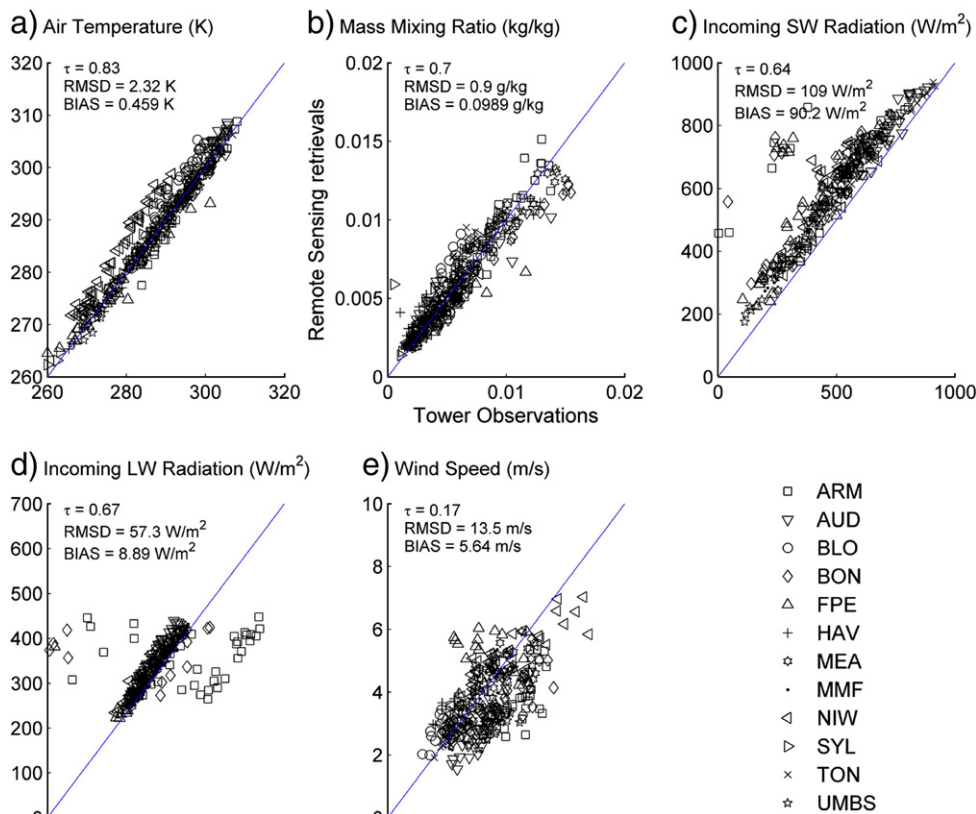


Fig. 5. Scatter plot (monthly mean) comparisons of (a) air temperature (T_{air}), (b) mass mixing ration (MMR), (c) incoming shortwave radiation (SW_{in}), (d) incoming longwave radiation (LWin), and (e) wind speed (WS), for years 2003 through 2006 over 12 flux towers.

at hourly time periods and thus were matched with the remote sensing based on the time of retrieval. Results show high scatter in the all the four variables. As discussed in Section 3, the bias in the incoming SW and LW radiation can be seen in the net radiation plot. Although the net radiation estimates correlate well with the in situ observations ($\tau = 0.72$), the bias ($\sim 125 \text{ W/m}^2$) and the root mean square difference (RMSD; $\sim 132 \text{ W/m}^2$) are higher, which we attribute to differences in albedo, surface temperature (not shown) and other spatial and temporal scale effects.

Comparisons between satellite retrieved latent heat flux and tower measured values raises a number of challenges and issues, which include the following. Firstly, the fluxes from remote sensing are instantaneous retrievals while the reported (available) flux tower data are normally aggregated over a 1-hour period. Our analysis of high temporal resolution (5 min) tower flux data shows indicative variability – especially near the EOS Aqua afternoon overpass – probably due to boundary layer clouds – that result in fast responses in the fluxes. Thus averaging the tower observations eliminates much of this high frequency ‘noise’, resulting in reporting intervals that range from 0.5 to 1 h (depending on site conditions and biome type). Complicating a comparison with retrievals from polar orbiting satellites is that the overpass times vary somewhat from orbit to orbit. For the Aqua afternoon overpass, it varies between 1300 h to 1400 h local standard time. These temporal scaling problems pose a major challenge to direct comparisons.

A second factor is the differences in spatial scales between the satellite footprints and the tower footprint, and the heterogeneity of the land surface within the satellite footprint (Kustas et al., 2004; Li et al., 2008). As indicated in Table 2, the scale of the satellite inputs ranged from 1 to 25 km, with most critical inputs at resolutions

$>10^1 \text{ km}$ while the eddy flux tower, in contrast, has a foot print of $<10^0 \text{ km}$, with the towers usually located in homogeneous land cover. To put these results into context, we consider the results of McCabe & Wood, 2006 who analyzed the spatial scaling effects from using land surface temperature inputs from Landsat (60 m), ASTER (90 m) and MODIS (1020 m) with the SEBS algorithm for the Walnut Creek (IA) catchment (area $\sim 53 \text{ km}^2$) that was the focus of the SMACEX'02 experiment. The landcover is a mix of corn and soybean, and they analyzed satellite data obtained between 10:30 and 11:12 am on July 1, 2002. The spatial variability (standard deviation and coefficient of variation (C_v) of the retrieved ET across the catchment from Landsat (ASTER) was 97 W/m^2 and 0.26 (103 W/m^2 and 0.26). When the high resolution remote sensing retrievals are averaged only to the overlying MODIS pixel centered on one of the 14 flux towers in the experiment, the within MODIS pixel variability (standard deviation and coefficient of variation) for Landsat (ASTER) was 85 W/m^2 and 0.23 (95 W/m^2 and 0.24). Thus, it can be concluded that for conditions where the radiation and meteorological conditions are homogeneous and landcover is constant, the variability in ET retrieval becomes stable somewhere just above 1 km with a C_v of about 0.25. In the current study, the remote sensing inputs are coarser (1000 m), suggesting that comparisons with single tower sites will always be problematic.

A third, long addressed issue with tower data is the lack of energy balance closure (see Twine et al., 2000 for an analysis of this problem). To show the mean annual closure residual, we calculate the mean closure $((LE_{\text{flux}} + H_{\text{flux}})/(R_{\text{net}} - G_{\text{flux}}))$ for all the towers (Table 3). With these issues in mind and the differences observed between the input datasets in Fig. 5, the comparisons observed in Fig. 6 can be put into context. Ferguson et al., 2010 found that the uncertainties in

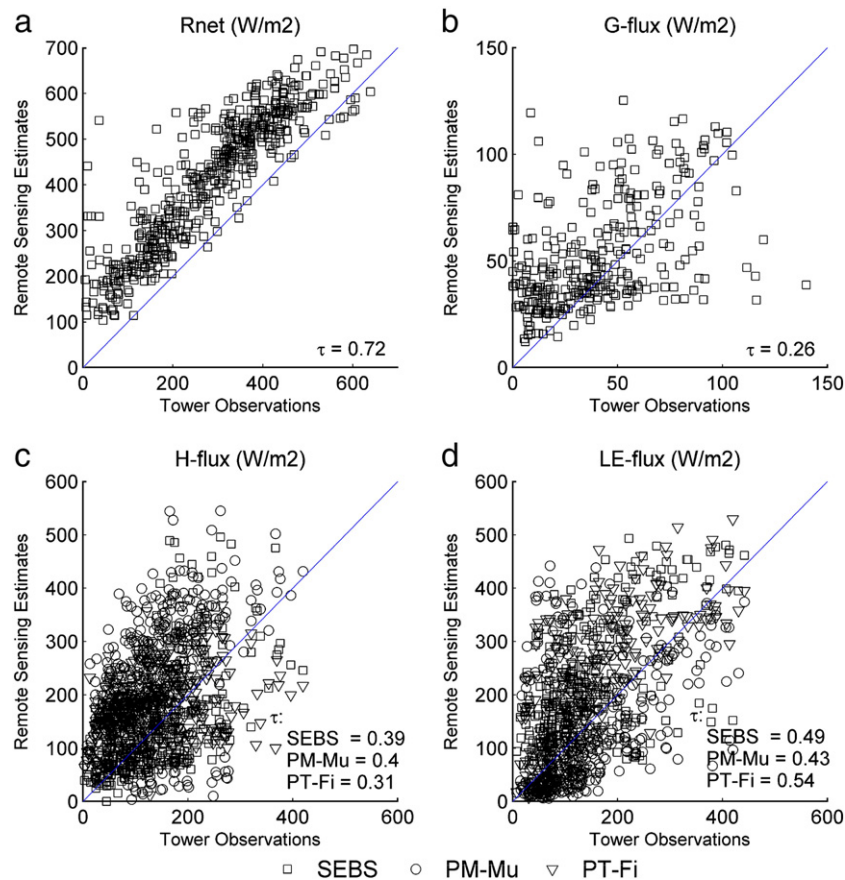


Fig. 6. Monthly mean remote sensing estimates (a) net radiation (Rnet); (b) soil heat flux (G-flux); (c) sensible heat flux (H-flux); and (d) latent heat flux (LE-flux), as compared with ground observations from flux towers for years 2003–2006. Tower fluxes averaged over the hour were used to compare with the instantaneous fluxes from remote sensing, considering that the satellites overpass time varied quite significantly.

vegetation parameterization and surface temperature (the affect of the latter on net radiation estimates) accounted for the maximum impact on the accuracy of the ET estimates. All the three models predict similar correlations for *LE* and *H* (instantaneous estimates), with *H* estimates showing more uncertainty than the *LE* estimates.

The instantaneous fluxes of latent- and sensible heat fluxes are scaled to equivalent daily ET and daily sensible heat flux, respectively, using the approach discussed in Section 3, and are further averaged (or summed) to monthly for comparison to flux tower estimates. Figs. 7 and 8 show the time series comparisons of the three remote

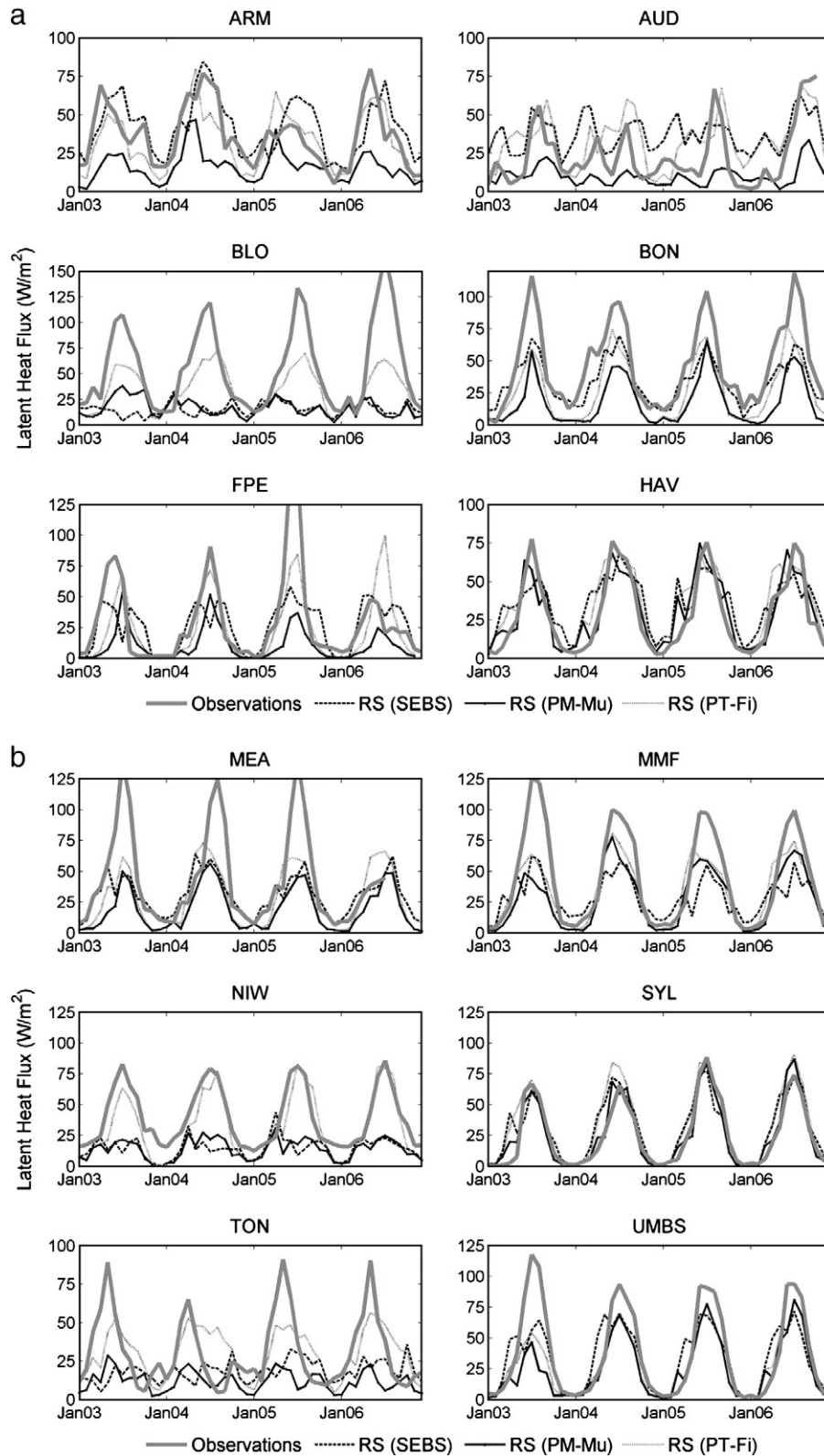


Fig. 7. a. Time series comparisons of 3 process based model ET (monthly total) estimates using remote sensing data. Observations from 12 eddy-flux towers are compared against the estimates. b. Continued from Fig. 7a.

sensing estimates of ET and H_{flux} to the tower fluxes. Level 4 (quality checked and gap filled data) Ameriflux data were used for the current comparisons. Table 4 presents the statistics of the comparisons at the individual towers. The mean correlation (Kendall's τ) for all sites, though the agreement varies for individual sites, is 0.51 (0.53), 0.55

(0.56) and 0.65 (0.53) for LE (H) from the SEBS, PM-Mu and PT-Fi models respectively. The mean RMS differences (RMSD) between the tower estimates of LE (H) ranged between 20 (35) and 27 (47) W/m^2 between the three models which correspond to 4.53 and 5.90% of the total annual evaporation across the towers.

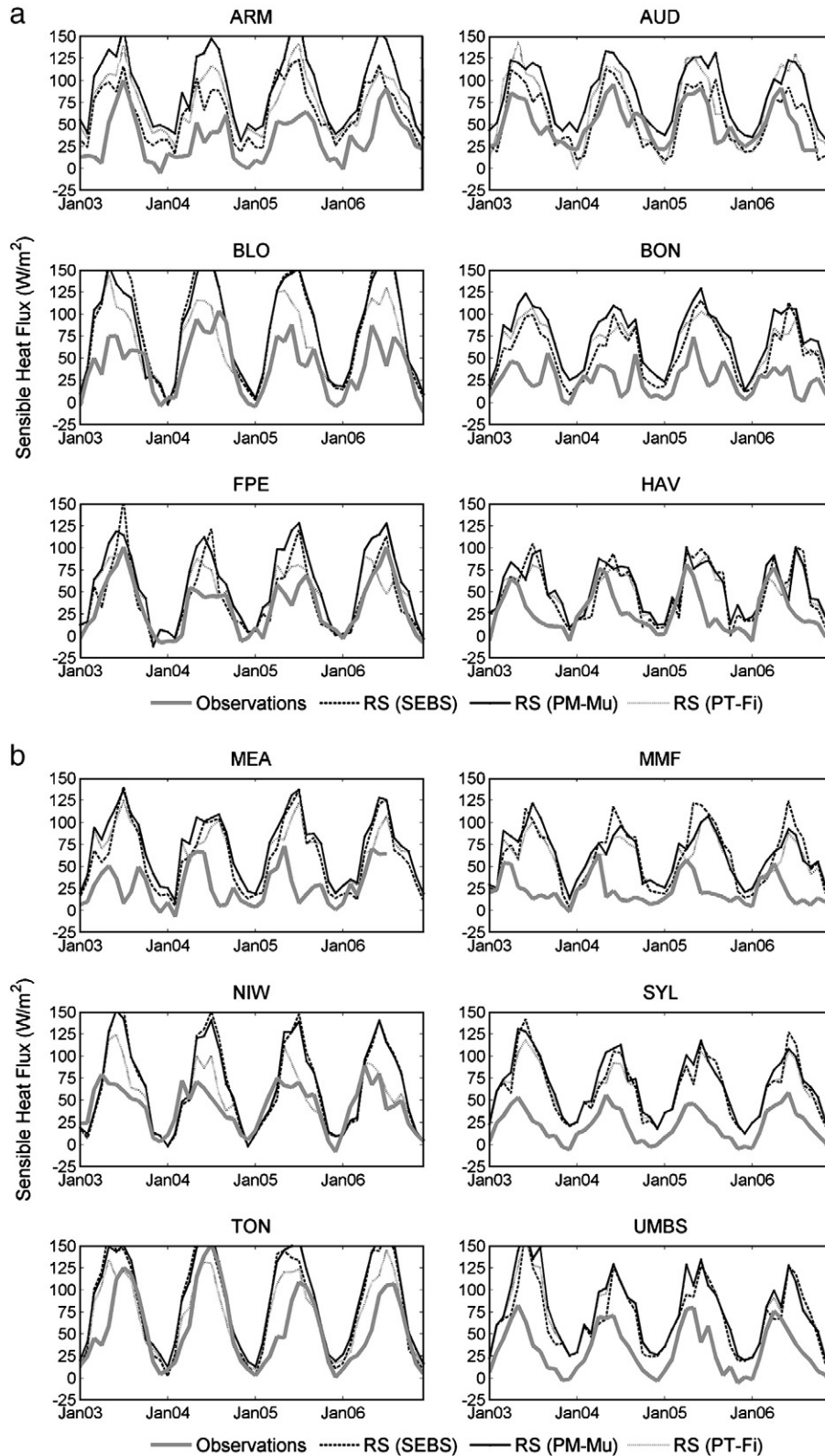


Fig. 8. a. Time series comparisons of 3 process based model H-flux (monthly mean) estimates using remote sensing data. Observations from 12 eddy-flux towers are compared against the estimates. b. Continued from Fig. 8a.

Table 4
Statistics of estimated surface fluxes against the eddy-flux tower observations.

Tower	Kendall's tau						Biome type
	Latent heat flux			Sensible heat flux			
	SEBS	PM-Mu	PT-Fi	SEBS	PM-Mu	PT-Fi	
ARM	0.55	0.53	0.60	0.52	0.54	0.57	Croplands
AUD	0.51	0.27	0.37	0.54	0.55	0.51	Grasslands
BLO	−0.11	0.22	0.72	0.70	0.68	0.63	Evergreen needleleaf forest
BON	0.77	0.61	0.71	0.45	0.45	0.41	Croplands
FPE	0.55	0.54	0.59	0.70	0.71	0.67	Grasslands
HAV	0.65	0.73	0.77	0.41	0.49	0.41	Deciduous broadleaf forest
MEA	0.77	0.69	0.67	0.40	0.43	0.34	Croplands
MMF	0.69	0.78	0.76	0.22	0.24	0.21	Deciduous broadleaf forest
NIW	0.32	0.55	0.71	0.56	0.59	0.64	Evergreen needleleaf forest
SYL	0.74	0.76	0.74	0.61	0.67	0.63	Mixed forests
TON	0.01	0.32	0.33	0.68	0.71	0.69	Woody savannas
UMBS	0.72	0.62	0.77	0.57	0.62	0.63	Deciduous broadleaf forest
Mean	0.51	0.55	0.65	0.53	0.56	0.53	
Tower	RMSD						Biome type
	Latent heat flux (W/m ²)			Sensible heat flux (W/m ²)			
	SEBS	PM-Mu	PT-Fi	SEBS	PM-Mu	PT-Fi	
ARM	15.71	25.32	13.24	38.04	62.22	44.23	Croplands
AUD	19.89	20.10	18.75	21.98	39.74	21.83	Grasslands
BLO	58.53	56.23	32.65	55.37	53.76	37.01	Evergreen needleleaf forest
BON	20.98	33.74	24.84	40.08	53.75	44.24	Croplands
FPE	28.41	32.78	24.26	23.26	31.76	21.44	Grasslands
HAV	16.14	10.78	12.20	35.23	34.32	31.65	Deciduous broadleaf forest
MEA	29.09	32.79	27.60	45.85	52.37	44.16	Croplands
MMF	29.61	25.73	21.28	51.68	48.07	42.54	Deciduous broadleaf forest
NIW	33.57	31.52	13.48	42.35	40.06	20.75	Evergreen needleleaf forest
SYL	12.60	7.41	13.07	46.60	48.97	42.21	Mixed forests
TON	27.22	27.15	19.39	41.14	42.76	29.03	Woody savannas
UMBS	21.45	22.91	19.75	44.35	50.22	47.23	Deciduous broadleaf forest
Mean	26.10	27.21	20.04	40.49	46.50	35.53	
Tower	BIAS						Biome type
	Latent heat flux (W/m ²)			Sensible heat flux (W/m ²)			
	SEBS	PM-Mu	PT-Fi	SEBS	PM-Mu	PT-Fi	
ARM	5.55	−20.22	−3.42	30.84	56.61	39.81	Croplands
AUD	13.86	−13.06	9.48	5.04	31.96	9.42	Grasslands
BLO	−39.90	−39.03	−21.83	43.19	42.33	25.12	Evergreen needleleaf forest
BON	−12.58	−28.71	−20.12	31.07	47.19	38.60	Croplands
FPE	−2.66	−18.42	−5.63	9.60	24.46	12.42	Grasslands
HAV	6.23	1.83	6.52	21.29	25.69	21.01	Deciduous broadleaf forest
MEA	−12.51	−24.04	−15.40	32.79	44.33	35.69	Croplands
MMF	−14.28	−15.78	−9.74	38.28	39.77	33.73	Deciduous broadleaf forest
NIW	−24.91	−25.08	−8.04	22.21	22.68	5.99	Evergreen needleleaf forest
SYL	4.57	0.42	6.67	40.54	44.70	38.44	Mixed forests
TON	−12.40	−18.84	−0.45	25.53	31.98	13.58	Woody savannas
UMBS	−3.91	−11.97	−9.50	35.38	43.43	40.97	Deciduous broadleaf forest
Mean	−7.74	−17.74	−5.95	27.98	37.93	26.23	

While a few of our towers overlap with those used by Mu et al. (2007), their observation period differs, which make comparisons difficult. Nonetheless, the mean absolute difference in the RMSD and bias statistics across the overlapping towers (BLO, BON, FPE, NIW, TON, and UMBS), between the PM-Mu estimates from the current study and Mu et al. (2007) estimates, are 5.20 W/m² and 2.0 W/m² respectively. Significant improvements in our PM-Mu based ET estimates were found over the BON, NIW, and TON towers. Although four of our towers match those used by Fisher et al., 2008, they did not provide the RMSD and bias for individual towers and furthermore the model was driven using in situ data.

Comparisons among the three models (Table 4) show the following results. For croplands (ARM, BON and MEA towers), grasslands (AUD and FPE towers) and woody savannas (TON tower), where the soil evaporation plays a dominant role, PT-Fi and SEBS estimates of ET showed the highest correlations against tower observations while PM-Mu estimates of H_{flux} showed the highest correlations. Over croplands,

it is observed that the SEBS and PT-Fi estimates match well (high correlation and low bias; see Fig. 7a and b) with the tower observations in winter time, there is a significant bias observed in the summer months, which corresponds to the growing season. The three cropland sites have a fetch which comprises of agricultural fields and thus have high ET during the summer time. On the other hand, when a remote sensing pixel is classified as croplands, it generally means that the pixel is dominated (>50% of the region) by cropland.

The RMSD and bias for all the models were within a small range. Over dense canopy, e.g. evergreen needleleaf forests (BLO and NIW towers) and deciduous broadleaf forests (HAV, MMF and UMBS towers), PT-Fi ET estimates showed the highest correlations. One final observation regarding the comparisons between the tower and remote sensing observation is the difference in the bias estimates between the LE and H flux estimates over the HAV, NIW and SYL towers. Although there is a low bias (<7 W/m²), for all the three models observed in the LE flux estimates over the HAV and SYL towers, the sensible heat flux estimates

are significantly different, with a range of 20–40 W/m² as compared with the observations. A similar observation is observed over the NIW tower for the PT-Fi estimates. One of the reasons, apart from the scale differences, could be associated with the energy balance closures over these towers. The closure estimates (Table 3) over these towers (≤ 0.80) suggest that the sum of the turbulent heat fluxes (H + LE) is less than the available energy (Rnet-G) which is a common observation over eddy flux towers (Twine et al., 2000). Considering the scale differences between the remote sensing estimates and tower footprint, differences between the input datasets and the uncertainties added by the temporal scaling (Ferguson et al., 2010), we conclude that the remote sensing estimates from the three models provide realistic quantification of the turbulent heat fluxes.

Energy balance residual could not be calculated using the Level 4 (gap filled and Ustar filtered records) Ameriflux data, due to the unavailability (i.e. not reported) of net radiation, which is only available in the Level 2 data).

4.2. Regional scale comparisons

The monthly remote sensing based ET estimates were also compared across 26 global river basins using a water budget analysis. Table 5 lists the 26 selected basins with the corresponding climatic zones and gauge locations. Since no observational evaporation dataset exists over the basins and observed basin discharge values are unavailable for the 2003–2006 period, the remote sensing estimates are compared to an inferred ET using the climatological values of precipitation, P_{clim} , and basin discharge, Q_{clim} as follows. The inferred (climatological) ET is calculated as $E_{inf} = P_{clim} - Q_{clim}$, under the assumption that over long time periods, the change in total water storage (soil moisture, lakes, wetlands, etc.) is negligible. The observed climatological discharge values for the basins were obtained from Global Runoff Data Center (GRDC) in Koblenz, Germany (Fekete et al., 2002). Even though the dataset is referred to as observed climatology, the data from each basin could range from a few years to up to ~100 years during the period 1901–2000. The time period (considered for the climatological product) for each basin is reported in Table 5. According to the station list catalogue reported by GRDC, only 11 out of the above 26 basins have reported data beyond year 2000, and only 4

beyond year 2003. The climatological data product is yet to be updated with data beyond year 2000.

To match the climatological product, we calculate a mean annual precipitation using the GPCP precipitation data for 100 years (1901–2000). Both the precipitation and runoff products are available at a 1° spatial resolution, so the three remote sensing based ET estimates were linearly scaled from 5 km to 1° using a box-averaging method, where >50% of the grid cells under a 1° domain are needed to upscale the estimates. The mean precipitation for the 100 years is compared (Fig. 9a) to the mean precipitation for 2003–2006. This comparison shows that the variability in precipitation was small with $\tau = 1.0$ and RMSD of 52 mm/year. We thus assume that the runoff ratio is not much different, ignoring any water management changes, for the two time periods (2003–2006 and 1901–2000). With that we compare the basin average estimates of remotely sensed ET to the inferred ET estimates (Fig. 9b), with τ ranging from 0.72 to 0.80; RMSD of 118 to 194 mm/year and bias ranging from –132 to 53 mm/year. RMSD (bias) found in the remotely sensed estimates is approximately 34% (10%) of the estimated mean annual (2003–2006) ET across the 26 basins. Results also show that the SEBS, PM-Mu and PT-Fi estimates complement each other across the basins, suggesting an opportunity for a multi-model ET estimate.

To put the remote sensing estimates into context, ET estimates (Sheffield and Wood, 2007) from the VIC land surface model (Cherkauer et al., 2003; Liang et al., 1994, 1996) and the ERA-interim reanalyses model (Simmons et al., 2007; Uppala et al., 2008) are also compared in Fig. 9b to the inferred ET estimates, with comparable values ($\tau = 0.72$ –0.89; RMSD ranging from 104 to 194 mm/year and bias –132 to 115 mm/year). Although VIC and ERA-interim showed high correlation and low RMSD, high biases were found in their estimates as compared to the inferred ET estimates. Analysis of the low-bias in the VIC evaporation estimates are due to high model estimates of basin discharge, which is being resolved through new global calibrations (Sheffield, personal communication). The ERA-interim estimates are consistent with results obtained by Betts et al. (2009), who compared the hydrometeorology of three American river basins (Amazon, Mississippi and Mackenzie rivers) against observations. Comparisons over the Mississippi and Mackenzie River basins showed that the ERA-interim estimates were higher than the observations. These high values, which are consistent over all the

Table 5
Selected river basins for basin scale comparisons of ET.

River basin	Gauge location	Climate	Upstream area (km ²)	GRDC time period
Amazon	Obidos, Brazil	Tropical	4,618,746	1928–1998
Mississippi	Vicksburg, USA	Mid-latitude rainy	2,964,254	1928–1983
Ganges	Paksey, Bangladesh	Mid-latitude rainy	1,000,000	1969–1975
Niger	Gaya, Niger	Semi-arid (north) tropical savannah (south)	940,050	1952–1990
Murray-Darling	Lock 9, Australia	Semi arid	1,000,000	1965–1984
Amur	Komsomolsk, Russia	Arctic	1,730,000	1932–1990
Mekong	Pakse, Laos	Tropical	545,000	1980–1991
Brahmaputra	Bahadurabad, Bangladesh	Mid-latitude rainy	636,130	1969–1992
Changjiang	Datong, China	Mid-latitude rainy	1,705,383	1922–1988
Danube	Drobeta-Turnu Severin, Romania	Mid-latitude rainy	576,232	1971–1983
Lena	Kyusyur, Russia	Arctic	2,430,000	1934–2000
Mackenzie	Norman Wells, Canada	Arctic	1,570,000	1943–1996
Ob	Salekhard, Russia	Arctic	2,430,000	1930–1999
Olenek	D/S of Pur River, Russia	Arctic	198,000	1965–1999
Parana	Corrientes, Argentina	Mid-latitude rainy	2,300,000	1904–1983
Pechora	Ust-Tsilma, Russia	Arctic	248,000	1932–1998
Severnaya Dvina	Ust-Pinega, Russia	Arctic	348,000	1881–1999
Volga	Volgograd, Russia	Mid-latitude rainy	1,360,000	1879–1984
Xi Jiang	Wuzhou, China	Mid-latitude rainy	329,705	1915–1986
Yana	Dzanghky, Russia	Arctic	216,000	1938–1989
Yenisei	Igarka, Russia	Arctic	2,440,000	1936–1999
Yukon	Ruby, United States	Arctic	670,810	1956–1984
Senegal	Bakel, Senegal	Arid hot/tropical	218,000	1904–1989
Indigirka	Vorontsovo, Russia	Arctic	305,000	1936–1998
Irrawaddy	Sagaing, Myanmar	Mid-latitude rainy	117,900	1978–1988
Kolyma	Sredne-Kolymsk, Russia	Arctic	361,000	1927–2000

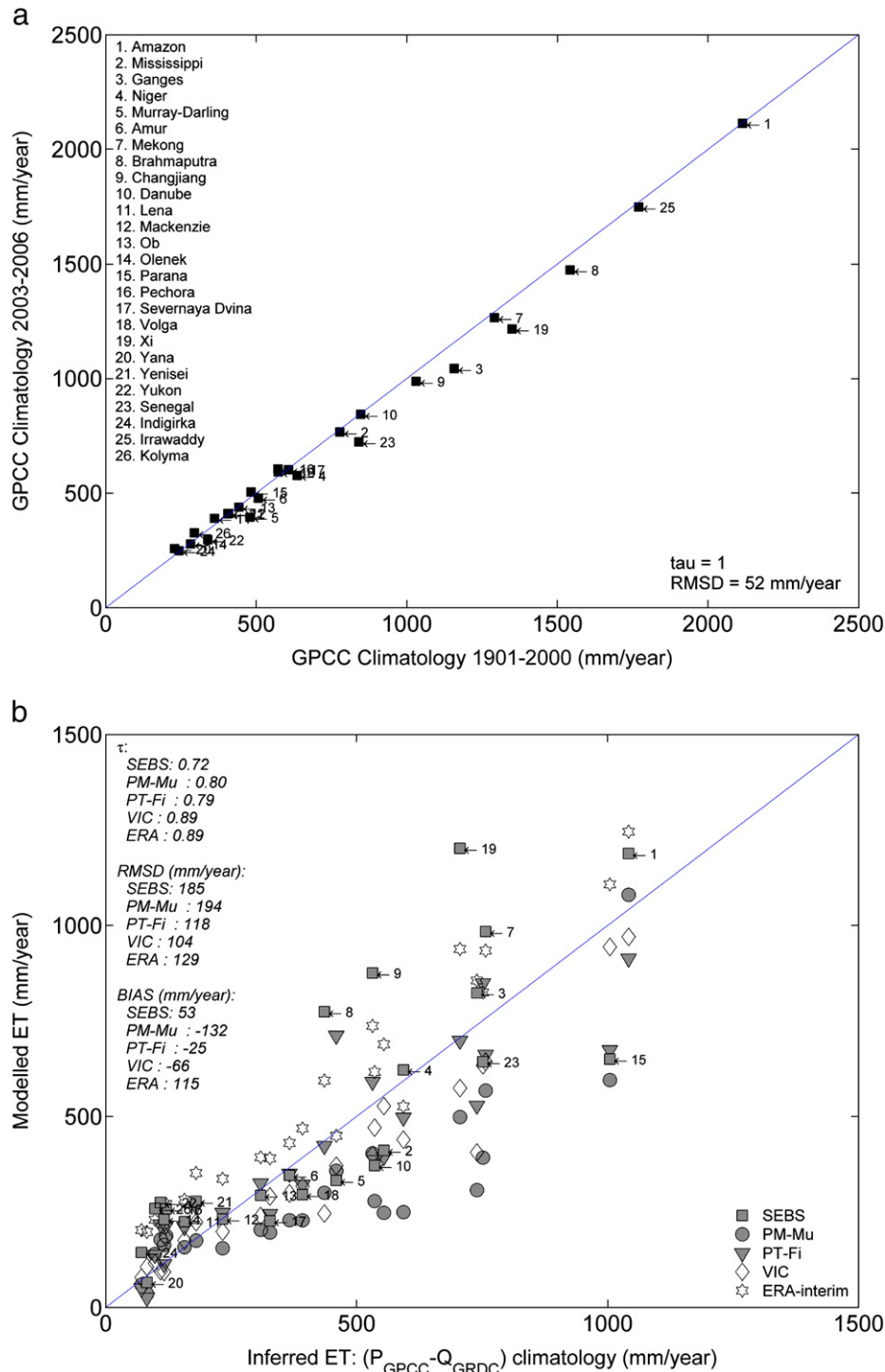


Fig. 9. (a) Comparison of the 100 year (1901–2000) precipitation climatology to the 4 year (2003–06) climatology over the 26 selected basins; (b) Annual ET comparisons over the 26 selected basins.

basins, are clearly seen in the scatter plot of Fig. 9b. Observational datasets for the Amazon basin are unavailable for the time period analyzed by Betts et al. (2009). Table 6 shows the comparisons of the basin scale ET estimates from the various models.

4.3. Continental/global scale comparisons

Global validation of evapotranspiration is problematic, considering that no observations are available at these spatial and temporal scales. The remote sensing ET products can be assessed at a global scale using

the same approach as in Section 4.2 for the large basins. Since observed discharge into the oceans from the global land area is unavailable, a GRDC composite runoff product (Fekete et al., 2002) is used. This product is based on a combination of the GRDC observations from over 1000 basins and a simple water balance model that extrapolates from the gauges basins to ungauged areas. As before, the remote sensing ET estimates, and estimates from VIC and ERA-interim, are compared to an inferred ET which is based on a (P-Q) climatology.

Fig. 10a shows the global latitudinal profiles, averaged for the years 2003–06, for the six evaporation datasets. A corresponding

Table 6
Comparison of the modeled and inferred ET estimates over the 26 basins.

River basin	inf-ET	SEBS	PM-Mu	PT-Fi	VIC	ERA
Amazon	1041.75	1188.04	1080.16	913.58	969.73	1244.93
Mississippi	554.16	411.17	247.69	393.69	526.84	688.44
Ganges	739.58	823.44	307.25	528.19	405.43	855.47
Niger	593.21	621.36	249.70	496.89	439.19	526.25
Murray-Darling	459.54	332.33	357.59	711.30	370.76	449.08
Amur	366.34	345.63	228.70	350.42	298.66	430.32
Mekong	757.01	983.90	567.69	661.27	642.92	933.84
Brahmaputra	435.67	773.81	299.84	422.82	245.64	593.86
Changjiang	531.72	875.71	403.29	590.93	399.46	736.80
Danube	535.71	371.46	278.43	385.44	470.67	616.18
Lena	157.11	224.68	157.67	210.79	175.50	281.74
Mackenzie	233.02	231.35	154.76	247.85	198.29	336.42
Ob	308.80	293.72	203.34	324.69	239.12	392.79
Olenek	116.43	230.90	163.41	113.23	92.55	216.95
Parana	1004.40	649.80	595.12	673.44	943.43	1107.24
Pechora	120.40	257.79	187.66	214.61	182.91	270.53
Severnaya Dvina	327.29	226.97	196.05	244.68	290.24	389.79
Volga	392.14	295.27	228.14	321.24	317.16	468.36
Xi jiang	705.80	1201.78	498.51	698.36	574.00	938.14
Yana	82.43	65.22	35.43	25.41	106.01	197.57
Yenisei	180.08	277.41	174.90	265.50	222.89	351.61
Yukon	109.51	274.72	177.37	217.17	94.72	267.58
Senegal	751.53	643.03	391.94	848.37	633.81	824.44
Indigirka	71.44	143.83	58.90	50.22	78.08	202.29
Irrawaddy	NaN	942.60	552.07	626.46	612.63	882.50
Kolyma	98.08	258.89	139.91	137.93	115.32	229.79

scatter plot of the latitudinal band estimates of the models versus the (P-Q) inferred estimates is shown in Fig. 10b. The three remote sensing estimates (SEBS, PM-Mu and PT-Fi) fall within the range of VIC and ERA-interim estimates with high tau (≥ 0.80) and lower bias as shown in Fig. 10b. It is our contention that the P-Q climatology, as an estimate for large basin and global ET over this period, is the best available estimate for evaluating our remote sensing estimates.

Remote sensing estimates from PT-Fi model show suppressed ET estimates between 12°S and 12°N latitudes. It was found by Mu et al. (2007) that the NDVI estimates exhibit scaling issues and saturated signals (owing to cloud cover) in the tropics where the land cover corresponds to high biomass conditions. These NDVI estimates are used by Ganguly et al. (2008) to create the global LAI dataset used in the current study, which we believe underestimates LAI due to this saturation. Furthermore, remote sensing estimates of LAI are usually lower than ground based measurements due to the lack of a clumping parameterization in the LAI models (Garrigues et al., 2008; Law & Waring, 1994). Since LAI estimates directly affect evapotranspiration estimates through the surface conductance (or resistance), parameterization, and evaporation of intercepted precipitation, which scales with LAI, an underestimation of LAI over the tropics will have the impact seen in Fig. 10a. The impact of intercepted precipitation on evaporation can be very high given the high precipitation rates over the tropical forests. We are unable to estimate the magnitude of this error from this source at this time. At this point, we find that the PT-Fi model gets most affected by the saturation of NDVI (and LAI), considering that the other two models do not use NDVI as an input.

Zonal monthly Hovmöller diagrams of total evapotranspiration over six continents are presented in Fig. 11. Antarctica is excluded from our current analysis. Here the total ET represents the average of the three models. Fig. 11 shows clearly the seasonal cycle of ET across the four year period, with some evidence of drought events across the continents. Some examples include the heat wave in Europe (July–August 2003), and the droughts over Amazon River basin (ARB; July–September 2005) and over the Australia (January–April 2005). Further analysis of the above events (not shown) revealed that the ET estimates were sensitive to the precipitation amounts, particularly in the water limited regions of Europe and Australia. The P-ET estimates (not shown) show values close to or below zero for the respective periods, thus confirming the droughts in the regions, and over the Amazon basin, we found reduced precipitation during the previous wet season, reduced ET during March–December period (see

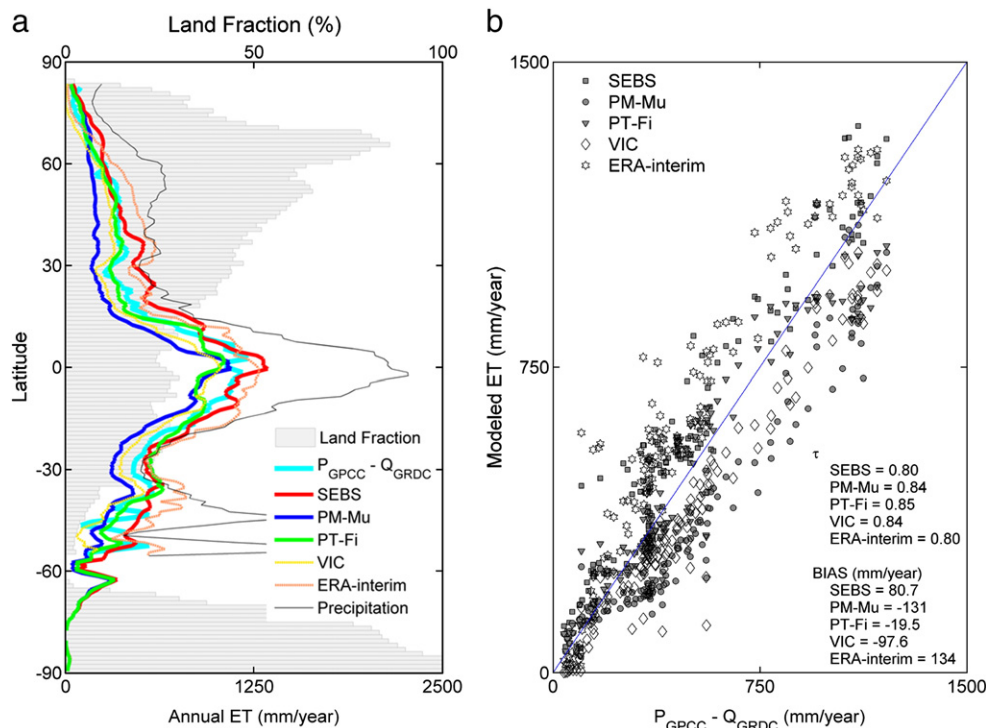


Fig. 10. (a) Global latitudinal profiles of annual ET; (b) Comparison of the latitudinal profiles of annual ET from 5 models to the inferred ET. Horizontal bars show the fraction of land per latitude band.

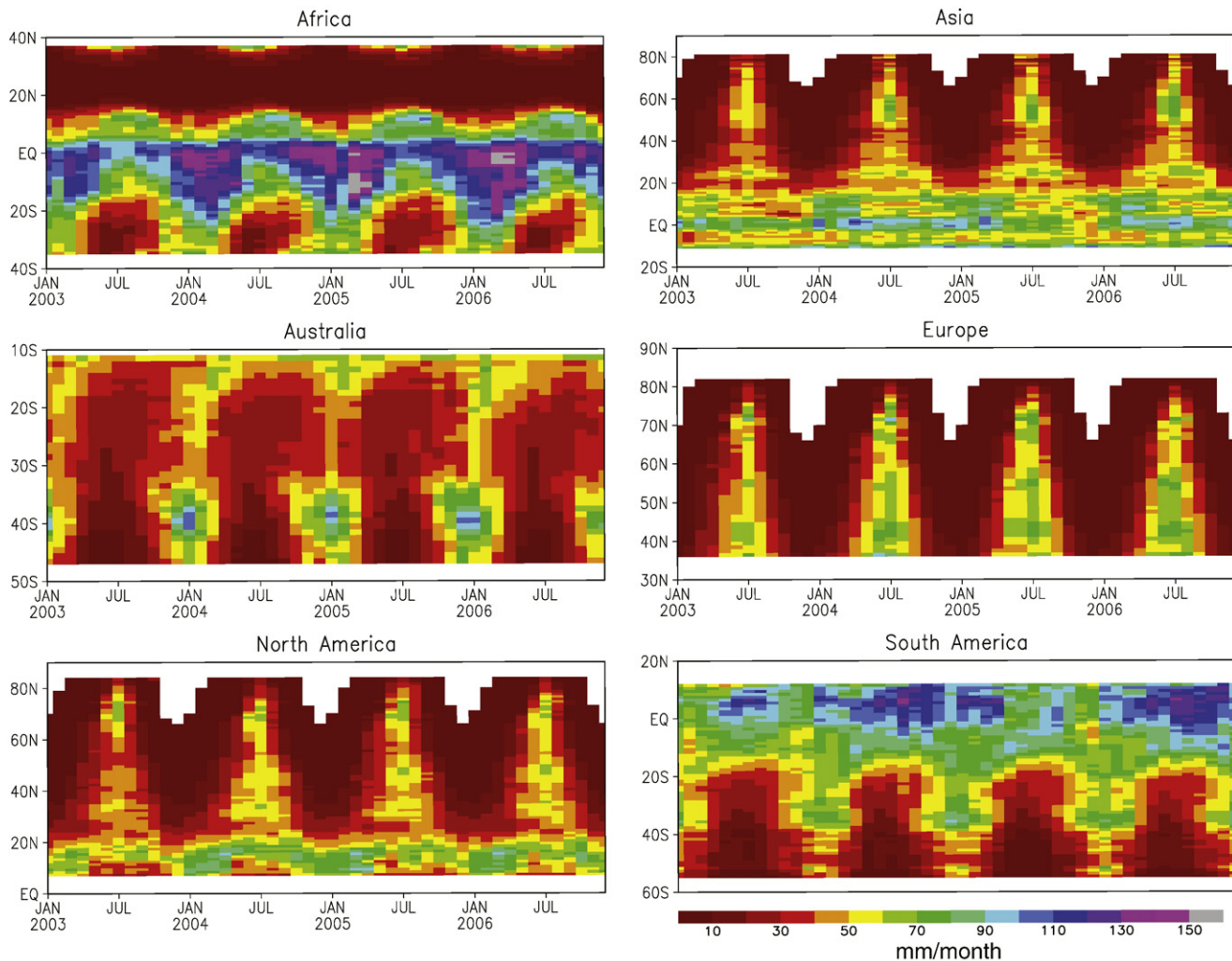


Fig. 11. Hovmöller diagram (monthly timescale) of the mean (of the 3 models used in the current study) evapotranspiration (mm/month) for the 6 continents.

Fig. 11) and negative values of P-ET for July–September 2005 – all indicators of drought throughout the basin.

Fig. 12 presents the interannual variation in ET as estimated by the SEBS, PM-Mu and PT-Fi algorithms. Although, a high spatial (Pearson's) correlation (>0.87) exists among the three model estimates, there exist differences among the estimates as was pointed out earlier (Fig. 10). More specifically, the PM-Mu algorithm provides a lower estimate for ET compared to SEBS and PT-Fi models. Some examples are over central Asia, Australia, Europe and western US. During the course of the comparisons, we found (not shown) that over water limited regions the ET estimates were not sensitive to the soil moisture dynamics of the region. Although relative humidity and thus vapor pressure deficit, along with vegetation characteristics, are assumed to reflect the dynamics of the soil moisture, Ferguson and Wood (in preparation) suggest that the degree to which soil moisture controls VPD varies as a function of dryness. The differences between the three process based ET estimates and their sensitivity to soil moisture are being investigated as part of the GEWEX Landflux initiative and will be the focus of a subsequent paper.

5. Summary and conclusions

The goal of the study was to develop a global dataset of evapotranspiration for climate studies using primarily NASA Earth Observing System remote sensing data. We use remote sensing datasets obtained from various sensors (AIRS, AVHRR, CERES and

MODIS onboard the NASA Aqua (EOS PM-Mu) and NOAA AVHRR polar orbiting satellites. Three process based models (Surface Energy Balance System – SEBS (Su, 2002); Penman–Monteith based algorithm – PM-Mu (Mu et al., 2007); and Priestley–Taylor based approach – PT-Fi (Fisher et al., 2008) were used to generate global instantaneous fluxes for the years 2003–2006. The instantaneous fluxes are then scaled to a daily value using the assumption of constant evaporative fraction over the day. The daily net radiation for the temporal scaling is obtained from the Surface Radiation Budget (SRB) dataset.

Evaluation of the coarse resolutions ET data has been an ongoing concern (Kalma et al., 2008) considering the fact that no robust methods or datasets exist at regional scales. To account for such issues, we evaluate our dataset at three different scales. First, the instantaneous fluxes are compared with eddy-flux observations from 12 towers, across the continental USA. Results show good agreement, with correlations of 0.43–0.54 in the instantaneous LE fluxes, between the remote sensing and tower fluxes, considering the various uncertainties that exist between input datasets due to spatial and temporal scaling issues. The daily ET values, summed up to the monthly scale, are compared with 12 flux towers with the results showing good correlations (0.51–0.65) and errors (RMSD: 20–27 W/m^2) within the expected range, again given input and scaling uncertainties. The scale mismatch between ET estimates based on remote sensing and tower observations makes their comparisons difficult and the evaluation of the remotely sensed estimates challenging. McCabe and Wood (2006) is

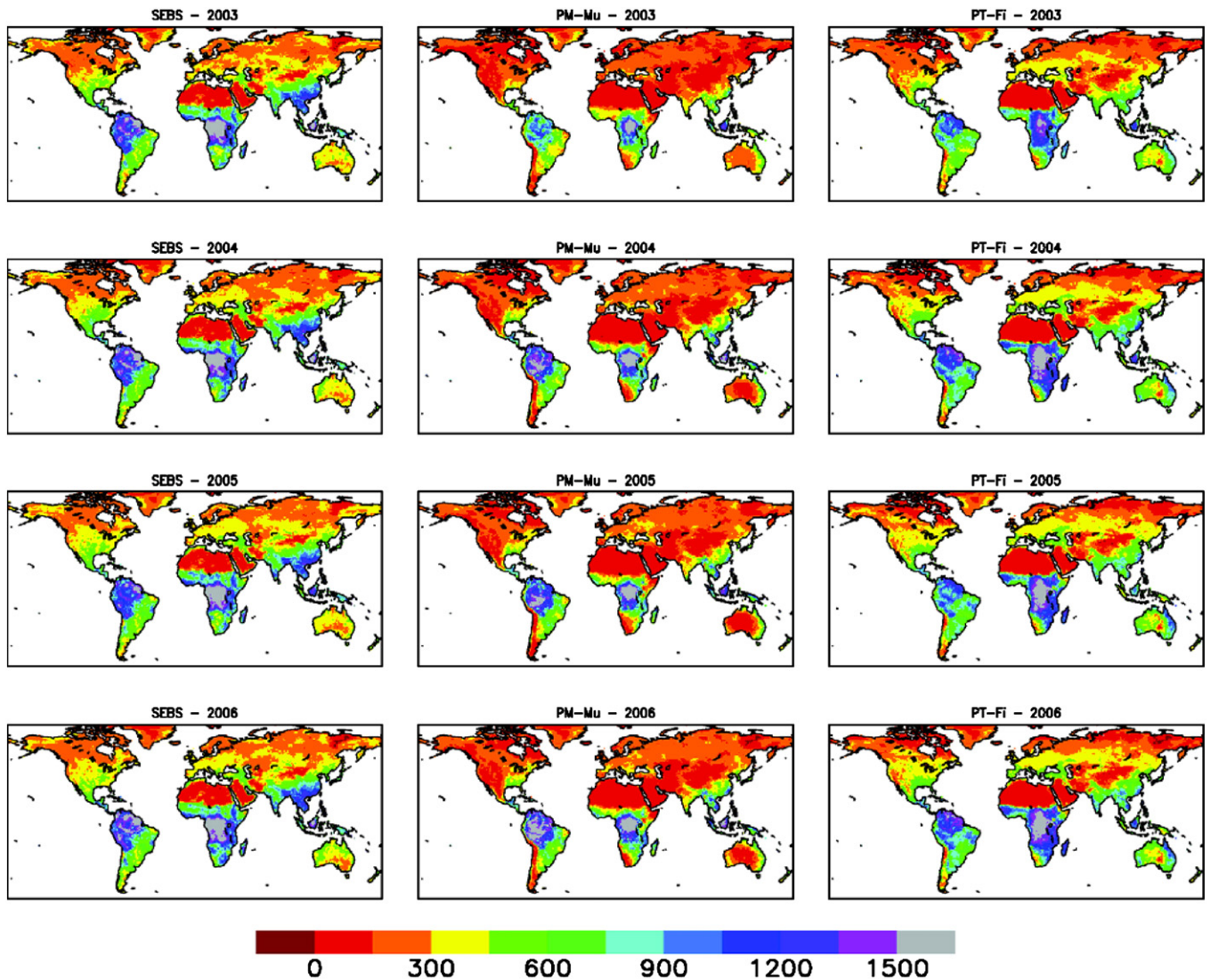


Fig. 12. Global annual ET for years 2003 through 2006.

perhaps the only research that has investigated the impact of errors in ET retrievals due to the scale of the remote sensing inputs, and the results of our study suggests that additional work along the lines of McCabe and Wood (2006) is required to better understand the errors in 'climate-scale' ET estimates as called for by the GEWEX Landflux initiative.

The second range of comparisons is carried out at spatial scales of $>10^4$ km² and at monthly to annual temporal scales. The basin scale comparisons indicate that the remote sensing estimates agree well with inferred evaporation calculated using climatological precipitation and basin discharge. The remote sensing estimates represent well, with correlations of 0.72–0.79 across the three model estimates, the basin scale inferred ET estimates. We find that the three models complement each other over basins across 6 climatic zones and varied vegetation types. This suggests the prospect for a multi-model analysis (e.g. Vinukollu et al., 2010) of remote sensing based ET estimates, which is planned as part of the on-going GEWEX Landflux study.

The third evaluation scale is a global comparison using latitudinal profiles. At this scale, the remote sensing estimates, when compared to the inferred ET from a (P-Q) analysis had higher Kendall's tau (0.80–0.85) and lower bias (mean bias ~ -23 mm/year) than the estimates from land surface and reanalysis models (VIC and ERA-interim). We further extend the analysis over six continents by plotting Hovmöller diagram of mean evapotranspiration from

averaging the three model estimates for 2003–2006. The seasonal cycle over the continents is well represented and the suppression of ET during major droughts in Europe, Australia and the Amazon are picked up. Nonetheless, the models, as formulated, appear to under-represent the sensitivity to soil moisture over water limited regions. The sensitivity of the ET estimates to the various input forcings and furthermore soil moisture is being investigated by the authors in a subsequent study. Overall, this points out the importance of analyzing the hydrological consistency of ET along with other water and energy budget components to further improve our understanding of coupled dynamic systems (McCabe et al., 2008b).

A primary focus of GEWEX and the NASA Energy and Water System (NEWS) study is to provide a quantitative description of water cycle variables over multiple decades. Although many variables pertaining to radiation, clouds, water vapor, precipitation, surface air temperature, river discharge, etc. are available for 20+ years, a need still exists to produce a global, multi-decadal land surface turbulent heat flux data product – the focus of the GEWEX Landflux project. The current study is a step in this direction, where we retrieved and analyzed a four years (2003–06) ET data set based on high quality NASA Earth Observing remote sensing products. Most of the remote sensing data for the current study is from sensors onboard the NASA Aqua satellite. A future step is to retrieve the turbulent heat fluxes using the global data compiled under the International Satellite

Land Surface Climatology Project (ISLSCP) as a contribution to the GEWEX Landflux initiative.

Acknowledgements

This work was jointly supported by NASA grants NNG04GQ32G “A Terrestrial Evaporation Data Product Using MODIS Data”; NNX08AN40A “Developing Consistent Earth System Data Records for the Global terrestrial Water Cycle”; and NNX09AK35G “Development and diagnostic analysis of a multi-decadal global evaporation product”. The data for the current study were obtained from NASA Langley Research Center Atmospheric Science Data Center, NASA/USGS Land Processes Distributed Active Archive Center, Goddard Earth Sciences Data and Information Services Center, Global Precipitation Climatology Center (GPCC), and the Global River Discharge Center (GRDC). We would like to thank Dr. Justin Sheffield and the European Center for Medium-Range Weather Forecasts (ECMWF) for the VIC land surface model and ERA-interim reanalysis datasets respectively. Lastly, this work would not have been possible without the use of the TIGRESS high performance computer center at Princeton University, which is jointly supported by the Princeton Institute for Computational Science and Engineering and the Princeton University Office of Information Technology (PU-OIT).

Appendix A. Methodology to calculate interception losses

A.1. Nomenclature

F_c	Fractional vegetation cover (amount of grid covered with vegetation)
f	fraction of vegetation in the vegetated part of the remote sensing grid
LAI	Leaf Area Index
n	fraction of precipitation that hits the ground un-intercepted, i.e. free throughfall
$S_{max}(t)$	Maximum storage capacity at time t
$S_c(t)$	Minimum quantity of precipitation required to attain canopy saturation at time t
$S(t)$	Actual storage at time t
$T_{drip}(t)$	throughfall (leaf drip) at time t
$E(t)$	Actual (canopy) evaporation at time t
$E_p(t)$	Potential (canopy) evaporation at time t

A.2. Procedure

1. Calculate the vegetation fraction, f and free throughfall fraction, n :

$$f = [1 - \exp(-0.5 \cdot LAI)]$$

(Kustas & Norman, 1996)

$$n = 1 - f$$

2. Calculate the maximum storage capacity of the canopy, S_{max} . Literature has revealed that this is a variable is a function of the leaf area index. However there are various empirical relationships that have been developed based on the biome type. See [de Jong and Jetten \(2007\)](#) for a detailed review of this parameter. For the current study, we consider the relationship developed by [Brisson et al. \(1998\)](#) which is also used in the Variable Infiltration Capacity land surface model.

$$S_{max}(t) = 0.2LAI$$

3. Calculate the value of the actual storage at time t , $S(t)$:

$$S(t) = \min[S_{max}(t), S(t-1) + (1-n)P(t)]$$

4. Calculate the throughfall, i.e. the water that drains from the leaves, at time t , $T_{drip}(t)$:

$$T_{drip}(t) = \max[S'(t-1) + (1-n)P(t) - S_{max}(t), 0]$$

5. Calculate the saturation capacity of the canopy at time t , $S_c(t)$:

$$S_c(t) = F_c \cdot S_{max}(t) \left[1 - e^{-P(t)/S_{max}(t)} \right]$$

(Kozak et al., 2007; Merriam, 1960)

6. If the actual storage is less than the saturation capacity of the canopy, then we assume that there will be no throughfall, i.e.

$$\text{if } [S'(t) < S_c(t)]; \text{ then } T_{drip}(t) = 0$$

7. Calculate the potential evaporation, $E_p(t)$, based on Priestley–Taylor algorithm:

$$E_p(t) = \alpha \frac{\Delta}{\Delta + \gamma} R_{net-veg}$$

8. If the actual storage is less than the saturation capacity of the canopy, then we scale the canopy evaporation, $E(t)$, as follows:

$$E(t) = \frac{S'(t)}{S_c(t)} \cdot E_p(t)$$

Otherwise,

$$E(t) = E_p(t)$$

9. When the canopy is completely saturated, i.e. $S(t) \geq S_c(t)$, we assume that the evapotranspiration process ceases,

$$ET(t) = 0$$

For $S(t) < S_c(t)$, we use the following expression for calculating the evapotranspiration (ET).

$$ET'(t) = \left(1 - \frac{S(t)}{S_c(t)} \right) ET(t)$$

Note that the evapotranspiration, $ET(t)$, is obtained from the three process models used in the current study, namely SEBS, PM-Mu and PT-Fi. Also it is to be noted that above value of ET is only over the vegetated part of the grid.

10. At the end of each time step, we revisit the actual storage by subtracting the canopy evaporation and throughfall, and pass the actual storage to the next time step:

$$S''(t) = S'(t) - E(t) - T_{drip}(t)$$

References

- Allen, R. G., Pruitt, W. O., Wright, J. L., Howell, T. A., Ventura, F., Snyder, R., Itenfisu, D., Steduto, P., Berengena, J., Yrisary, J. B., Smith, M., Pereira, L. S., Raes, D., Perrier, A., Alves, I., Walter, I., & Elliott, R. (2006). A recommendation on standardized surface resistance for hourly calculation of reference ETO by the FAO56 Penman–Monteith method. *Agricultural Water Management*, 81, 1–22.
- Allen, R. G., Tasumi, M., & Trezza, R. (2007). Satellite-based energy balance for mapping evapotranspiration with internalized calibration (METRIC) – Model. *Journal of Irrigation and Drainage Engineering-ASCE*, 133, 380–394.
- Anderson, M. C., Kustas, W. P., & Norman, J. M. (2003). Upscaling and downscaling – A regional view of the soil–plant–atmosphere continuum. *Agronomy Journal*, 95, 1408–1423.
- Anderson, M. C., Norman, J. M., Diak, G. R., Kustas, W. P., & Mecikalski, J. R. (1997). A two-source time-integrated model for estimating surface fluxes using thermal infrared remote sensing. *Remote Sensing of Environment*, 60, 195–216.
- Anderson, M. C., Norman, J. M., Mecikalski, J. R., Otkin, J. A., & Kustas, W. P. (2007). A climatological study of evapotranspiration and moisture stress across the

- continental United States based on thermal remote sensing: 1. Model formulation. *Journal of Geophysical Research-Atmospheres*, 112.
- Baldocchi, D., Falge, E., Gu, L. H., Olson, R., Hollinger, D., Running, S., Anthoni, P., Bernhofer, C., Davis, K., Evans, R., Fuentes, J., Goldstein, A., Katul, G., Law, B., Lee, X. H., Malhi, Y., Meyers, T., Munger, W., Oechel, W., U, K.T.P., Pilegaard, K., Schmid, H. P., Valentini, R., Verma, S., Vesala, T., Wilson, K., & Wofsy, S. (2001). FLUXNET: A new tool to study the temporal and spatial variability of ecosystem-scale carbon dioxide, water vapor, and energy flux densities. *Bulletin of the American Meteorological Society*, 82, 2415–2434.
- Baldocchi, D. D., Hicks, B. B., & Meyers, T. P. (1988). Measuring biosphere-atmosphere exchanges of biologically related gases with micrometeorological methods. *Ecology*, 69, 1331–1340.
- Ball, J. T., Woodrow, I. E., & Berry, J. A. (1987). A model predicting stomatal conductance and its contribution to the control of photosynthesis under different environmental conditions. In J. Biggins (Ed.), *7th international congress on photosynthesis* (pp. 221–224). Dordrecht, The Netherlands: Martinus Nijhoff.
- Barton, I. J. (1979). Parameterization of the evaporation from non-saturated surfaces. *Journal of Applied Meteorology*, 18, 43–47.
- Bastiaanssen, W. G. M., Menenti, M., Feddes, R. A., & Holtslag, A. A. M. (1998). A remote sensing surface energy balance algorithm for land (SEBAL) – 1. Formulation. *Journal of Hydrology*, 213, 198–212.
- Bennett, W. B., Wang, J. F., & Bras, R. L. (2008). Estimation of global ground heat flux. *Journal of Hydrometeorology*, 9, 744–759.
- Betts, A. K., Kohler, M., & Zhang, Y. C. (2009). Comparison of river basin hydrodrometeorology in ERA-Interim and ERA-40 reanalyses with observations. *Journal of Geophysical Research-Atmospheres*, 114.
- Bintanja, R. (1998). The contribution of snowdrift sublimation to the surface mass balance of Antarctica. *Annals of Glaciology*, 27, 251–259.
- Blaney, H. F., & Criddle, W. D. (1950). *Determining water requirements in irrigated areas from climatological and irrigation data* (pp. 48). : US Department of Agriculture Soil Conservation Service.
- Blumel, K. (1999). A simple formula for estimation of the roughness length for heat transfer over partly vegetated surfaces. *Journal of Applied Meteorology*, 38, 814–829.
- Bowling, L. C., Pomeroy, J. W., & Lettenmaier, D. P. (2004). Parameterization of blowing-snow sublimation in a macroscale hydrology model. *Journal of Hydrometeorology*, 5, 745–762.
- Brisson, N., Mary, B., Ripoche, D., Jeuffroy, M. H., Ruget, F., Nicoulaud, B., Gate, P., Devienne-Barret, F., Antonioletti, R., Durr, C., Richard, G., Beaudoin, N., Recous, S., Tayot, X., Plenet, D., Cellier, P., Machet, J. M., Meynard, J. M., & Delecolle, R. (1998). STICS: a generic model for the simulation of crops and their water and nitrogen balances. I. Theory and parameterization applied to wheat and corn. *Agronomie*, 18, 311–346.
- Brutsaert, W. (1982). *Evaporation into the atmosphere: Theory, History and Applications* (1st ed.). Springer.
- Burgy, R. H., & Pomeroy, C. R. (1958). Interception losses in grassy vegetation. *Transactions of the American Geophysical Union*, 39, 1095–1100.
- Calder, I. R. (1990). *Evaporation in the uplands*. Chichester; New York: Wiley.
- Carlyle-Moses, D. E., & Price, A. G. (1999). An evaluation of the Gash interception model in a northern hardwood stand. *Journal of Hydrology*, 214, 103–110.
- Castellvi, F., Stockle, C. O., Perez, P. J., & Ibanez, M. (2001). Comparison of methods for applying the Priestley-Taylor equation at a regional scale. *Hydrological Processes*, 15, 1609–1620.
- Cherkauer, K. A., Bowling, L. C., & Lettenmaier, D. P. (2003). Variable infiltration capacity cold land process model updates. *Global and Planetary Change*, 38, 151–159.
- Cleugh, H. A., Leuning, R., Mu, Q. Z., & Running, S. W. (2007). Regional evaporation estimates from flux tower and MODIS satellite data. *Remote Sensing of Environment*, 106, 285–304.
- Crago, R. D. (1996). Comparison of the evaporative fraction and the Priestley-Taylor alpha for parameterizing daytime evaporation. *Water Resources Research*, 32, 1403–1409.
- Crago, R., & Brutsaert, W. (1996). Daytime evaporation and the self-preservation of the evaporative fraction and the Bowen ratio. *Journal of Hydrology*, 178, 241–255.
- Dalton, J. (1802). Experimental essays in the constitution of mixed gases; on the force of steam of vapor from waters and other liquids in different temperatures, both in a torricellian vacuum and in air; on evaporation; and on the expansion of gases by heat. *Memoirs of the Manchester Lit. & Phil. Soc.*, 535–602.
- Dang, Q. L., Margolis, H. A., Coyea, M. R., Sy, M., & Collatz, G. J. (1997). Regulation of branch-level gas exchange of boreal trees: Roles of shoot water potential and vapor pressure difference. *Tree Physiology*, 17, 521–535.
- Davies, J. A., & Allen, C. D. (1973). Equilibrium, potential and actual evaporation from cropped surfaces in southern Ontario. *Journal of Applied Meteorology*, 12, 649–657.
- Debruin, H. A. R., & Keijman, J. Q. (1979). Priestley-Taylor evaporation model applied to a large, shallow lake in the Netherlands. *Journal of Applied Meteorology*, 18, 898–903.
- de Jong, S. M., & Jetten, V. G. (2007). Estimating spatial patterns of rainfall interception from remotely sensed vegetation indices and spectral mixture analysis. *International Journal of Geographical Information Science*, 21, 529–545.
- Dery, S. J., & Yau, M. K. (2001). Simulation of blowing snow in the Canadian Arctic using a double-moment model. *Boundary-Layer Meteorology*, 99, 297–316.
- Diawara, A., Loustau, D., & Berbigier, P. (1991). Comparison of 2 methods for estimating the evaporation of a *Pinus pinaster* (Ait) stand – Sap flow and energy-balance with sensible heat-flux measurements by an eddy covariance method. *Agricultural and Forest Meteorology*, 54, 49–66.
- Dickinson, R. E., Shaikh, M., Bryant, R., & Graumlich, L. (1998). Interactive canopies for a climate model. *Journal of Climate*, 11, 2823–2836.
- Dolman, A. J., Gash, J. H. C., Roberts, J., & Shuttleworth, W. J. (1991). Stomatal and surface conductance of tropical rain-forest. *Agricultural and Forest Meteorology*, 54, 303–318.
- Essery, R. (2001). Spatial statistics of windflow and blowing-snow fluxes over complex topography. *Boundary-Layer Meteorology*, 100, 131–147.
- Essery, R., Li, L., & Pomeroy, J. (1999). A distributed model of blowing snow over complex terrain. *Hydrological Processes*, 13, 2423–2438.
- Fekete, B., Vörösmarty, C., & Grabs, W. (2002). Global composite runoff fields on observed river discharge and simulated water balances. In Koblenz (Ed.), *Water System Analysis Group*. : University of New Hampshire, and Global Runoff Data Centre, Federal Institute of Hydrology.
- Ferguson, C. R., Sheffield, J., Wood, E. F., & Gao, H. L. (2010). Quantifying uncertainty in a remote sensing-based estimate of evapotranspiration over continental USA. *International Journal of Remote Sensing*, 31, 3821–3865.
- Ferguson, C. R., & Wood, E. F. (in preparation). Consensus view of global soil moisture-precipitation feedback strength from models and satellite remote sensing. *Hydrology and Earth System Sciences*.
- Ferguson, C. R., & Wood, E. F. (2010). An evaluation of satellite remote-sensing data products for land surface hydrology: Atmospheric Infrared Sounder (AIRS). *Journal of Hydrometeorology*. Early online.
- Fisher, J. B., DeBiase, T. A., Qi, Y., Xu, M., & Goldstein, A. H. (2005). Evapotranspiration models compared on a Sierra Nevada forest ecosystem. *Environmental Modelling and Software*, 20, 783–796.
- Fisher, J. B., Malhi, Y., Bonal, D., Da Rocha, H. R., De Araujo, A. C., Gamon, M., Goulden, M. L., Hirano, T., Huete, A. R., Kondo, H., Kumagai, T., Loeschner, H. W., Miller, S., Nobre, A. D., Nouvellon, Y., Oberbauer, S. F., Panuthai, S., Rouspard, O., Saleska, S., Tanaka, K., Tanaka, N., Tu, K. P., & Von Randow, C. (2009). The land-atmosphere water flux in the tropics. *Global Change Biology*, 15, 2694–2714.
- Fisher, J. B., Tu, K. P., & Baldocchi, D. D. (2008). Global estimates of the land-atmosphere water flux based on monthly AVHRR and ISLSCP-II data, validated at 16 FLUXNET sites. *Remote Sensing of Environment*, 112, 901–919.
- Fisher, J. B., Whittaker, R., & Malhi, Y. (2011). ET come home: potential evapotranspiration in geographical ecology. *Global Ecology and Biogeography*, 20, 1–18.
- Flint, A. L., & Childs, S. W. (1991). Use of the Priestley-Taylor evaporation equation for soil-water limited conditions in a small forest clear-cut. *Agricultural and Forest Meteorology*, 56, 247–260.
- Frempong, E. (1983). Diel aspects of the thermal structure and energy budget of a small English lake. *Freshwater Biology*, 13, 89–102.
- Ganguly, S., Schull, M. A., Samanta, A., Shabanov, N. V., Milesi, C., Nemani, R. R., Knyazikhin, Y., & Myneni, R. B. (2008). Generating vegetation leaf area index earth system data record from multiple sensors. Part 1: Theory. *Remote Sensing of Environment*, 112, 4333–4343.
- Garrigues, S., Lacaze, R., Baret, F., Morisette, J. T., Weiss, M., Nickeson, J. E., Fernandes, R., Plummer, S., Shabanov, N. V., Myneni, R. B., Knyazikhin, Y., & Yang, W. (2008). Validation and intercomparison of global Leaf Area Index products derived from remote sensing data. *Journal of Geophysical Research-Geosciences*, 113.
- Gash, J. H. C. (1979). Analytical model of rainfall interception by forests. *Quarterly Journal Royal Meteorological Society*, 105, 43–55.
- Gavilan, P., Berengena, J., & Allen, R. G. (2007). Measuring versus estimating net radiation and soil heat flux: Impact on Penman-Monteith reference ET estimates in semiarid regions. *Agricultural Water Management*, 89, 275–286.
- Green, A. E., Clothier, B. E., Kerr, J. P., & Scotter, D. R. (1984). Evapotranspiration from pasture – A comparison of lysimeter and Bowen-ratio measurements with Priestley-Taylor estimates. *New Zealand Journal of Agricultural Research*, 27, 321–327.
- Guo, X. F., Zhang, H. S., Kang, L., Du, J. L., Li, W. B., & Zhu, Y. J. (2007). Quality control and flux gap filling strategy for Bowen ratio method: revisiting the Priestley – Taylor evaporation model. *Environmental Fluid Mechanics*, 7, 421–437.
- Gupta, S. K., Darnell, W. L., & Wilber, A. C. (1992). A parameterization for longwave surface radiation from satellite data – Recent improvements. *Journal of Applied Meteorology*, 31, 1361–1367.
- Gupta, S. K., Kratz, D. P., Stackhouse, P. W., & Wilber, A. C. (2001). *The Langley Parameterized Shortwave Algorithm (LPSA) for Surface Radiation Budget Studies* (pp. 31). : NASA.
- Gutman, G., & Ignatov, A. (1998). The derivation of the green vegetation fraction from NOAA/AVHRR data for use in numerical weather prediction models. *International Journal of Remote Sensing*, 19, 1533–1543.
- Hargreaves, G. H. (1975). Moisture availability and crop production. *Transactions of the Asae*, 18, 980–984.
- Huffman, G. J., Adler, R. F., Morrissey, M. M., Bolvin, D. T., Curtis, S., Joyce, R., McGavock, B., & Susskind, J. (2001). Global precipitation at one-degree daily resolution from multisatellite observations. *Journal of Hydrometeorology*, 2, 36–50.
- Irmak, S., Howell, T. A., Allen, R. G., Payero, J. O., & Martin, D. L. (2005). Standardized ASCE Penman-Monteith: Impact of sum-of-hourly vs. 24-hour timestep computations at reference weather station sites. *Transactions of the Asae*, 48, 1063–1077.
- Jarvis, P. G. (1976). The interpretation of the variations in leaf water potential and stomatal conductance found in canopies in the field. *Philosophical Transactions of the Royal Society of London Series B, Biological Sciences*, 273, 593–610.
- Jetten, V. G. (1996). Interception of tropical rain forest: Performance of a canopy water balance model. *Hydrological Processes*, 10, 671–685.
- Jia, L., Su, Z. B., van den Hurk, B., Menenti, M., Moene, A., De Bruin, H. A. R., Yrisarry, J. J. B., Ibanez, M., & Cuesta, A. (2003). Estimation of sensible heat flux using the Surface Energy Balance System (SEBS) and ATSR measurements. *Physics and Chemistry of the Earth*, 28, 75–88.
- Jimenez, C., Prigent, C., Mueller, B., Seneviratne, S. I., McCabe, M. F., Wood, E. F., Rossow, W. B., Balsamo, G., Betts, A. K., Dirmeyer, P., Fisher, J. B., Jung, M., Kanamitsu, M.,

- Reichle, R.H., Reichstein, M., Rodell, M., Sheffield, J., Tu, K., & Wang, K. (in press). Global inter-comparison of 12 land surface heat flux estimates. *Journal of Geophysical Research*, 2010J014545.
- Jin, Y. F., Schaaf, C. B., Woodcock, C. E., Gao, F., Li, X. W., Strahler, A. H., Lucht, W., & Liang, S. L. (2003). Consistency of MODIS surface bidirectional reflectance distribution function and albedo retrievals: 2. Validation. *Journal of Geophysical Research-Atmospheres*, 108.
- Kalma, J. D., McVicar, T. R., & McCabe, M. F. (2008). Estimating land surface evaporation: A review of methods using remotely sensed surface temperature data. *Surveys in Geophysics*, 29, 421–469.
- Kawamitsu, Y., Yoda, S., & Agata, W. (1993). Humidity pretreatment affects the responses of stomata and CO₂ assimilation to vapor-pressure difference in C-3 and C-4 plants. *Plant & Cell Physiology*, 34, 113–119.
- Kozak, J. A., Ahuja, L. R., Green, T. R., & Ma, L. W. (2007). Modelling crop canopy and residue rainfall interception effects on soil hydrological components for semi-arid agriculture. *Hydrological Processes*, 21, 229–241.
- Kustas, W. P., & Daughtry, C. S. T. (1990). Estimation of the soil heat-flux net-radiation ratio from spectral data. *Agricultural and Forest Meteorology*, 49, 205–223.
- Kustas, W. P., Li, F., Jackson, T. J., Prueger, J. H., MacPherson, J. L., & Wolde, M. (2004). Effects of remote sensing pixel resolution on modeled energy flux variability of croplands in Iowa. *Remote Sensing of Environment*, 92, 535–547.
- Kustas, W. P., & Norman, J. M. (1996). Use of remote sensing for evapotranspiration monitoring over land surfaces. *Hydrological Sciences Journal-Journal Des Sciences Hydrologiques*, 41, 495–516.
- Law, B. E., & Waring, R. H. (1994). Remote-sensing of leaf-area index and radiation intercepted by understory vegetation. *Ecological Applications*, 4, 272–279.
- Leuning, R. (1995). A critical-appraisal of a combined stomatal-photosynthesis model for C-3 plants. *Plant, Cell & Environment*, 18, 339–355.
- Leuning, R., Denmead, O. T., Lang, A. R. G., & Ohtaki, E. (1982). Effects of heat and water-vapor transport on eddy covariance measurement of CO₂ fluxes. *Boundary-Layer Meteorology*, 23, 209–222.
- Lhomme, J. P. (1997). An examination of the Priestley–Taylor equation using a convective boundary layer model. *Water Resources Research*, 33, 2571–2578.
- Li, F. Q., Kustas, W. P., Anderson, M. C., Prueger, J. H., & Scott, R. L. (2008). Effect of remote sensing spatial resolution on interpreting tower-based flux observations. *Remote Sensing of Environment*, 112, 337–349.
- Liang, S. L., Fang, H. L., Chen, M. Z., Shuey, C. J., Walhall, C., Daughtry, C., Morissette, J., Schaaf, C., & Strahler, A. (2002). Validating MODIS land surface reflectance and albedo products: methods and preliminary results. *Remote Sensing of Environment*, 83, 149–162.
- Liang, X., Lettenmaier, D. P., & Wood, E. F. (1996). One-dimensional statistical dynamic representation of subgrid spatial variability of precipitation in the two-layer variable infiltration capacity model. *Journal of Geophysical Research-Atmospheres*, 101, 21403–21422.
- Liang, X., Lettenmaier, D. P., Wood, E. F., & Burges, S. J. (1994). A simple hydrologically based model of land-surface water and energy fluxes for general-circulation models. *Journal of Geophysical Research-Atmospheres*, 99, 14415–14428.
- Liston, G. E., & Sturm, M. (1998). A snow-transport model for complex terrain. *Journal of Glaciology*, 44, 498–516.
- Liu, X. Y., & Lin, E. (2005). Performance of the Priestley–Taylor equation in the semiarid climate of North China. *Agricultural Water Management*, 71, 1–17.
- Lundberg, A., & Halldin, S. (2001). Snow interception evaporation. Review of measurement techniques, processes, and models. *Theoretical and Applied Climatology*, 70, 117–133.
- Marsden, B. J., Lieffers, V. J., & Zwiazek, J. J. (1996). The effect of humidity on photosynthesis and water relations of white spruce seedlings during the early establishment phase. *Canadian Journal of Forest Research-Revue Canadienne De Recherche Forestiere*, 26, 1015–1021.
- Massman, W. J. (1999). A model study of kB(H)(–1) for vegetated surfaces using 'localized near-field' Lagrangian theory. *Journal of Hydrology*, 223, 27–43.
- Mccabe, M. F., Balick, L. K., Theiler, J., Gillespie, A. R., & Mushkin, A. (2008). Linear mixing in thermal infrared temperature retrieval. *International Journal of Remote Sensing*, 29, 5047–5061.
- Mccabe, M. F., & Wood, E. F. (2006). Scale influences on the remote estimation of evapotranspiration using multiple satellite sensors. *Remote Sensing of Environment*, 105, 271–285.
- Mccabe, M. F., Wood, E. F., Wojcik, R., Pan, M., Sheffield, J., Gao, H., & Su, H. (2008). Hydrological consistency using multi-sensor remote sensing data for water and energy cycle studies. *Remote Sensing of Environment*, 112, 430–444.
- Menenti, M., & Choudhury, B. J. (1993). Parameterization of land surface evaporation by means of location dependent potential evaporation and surface temperature range. In H. J. Bolle, R. A. Feddes, & J. D. Kalma (Eds.), *Exchange processes at the land surface for a range of space and time scales*. Yokohama: IAHS.
- Merriam, R. A. (1960). A note on the interception loss equation. *Journal of Geophysical Research*, 65, 3850–3851.
- Miralles, D. G., Gash, J. H., Holmes, T. R. H., de Jeu, R. A. M., & Dolman, A. J. (2010). Global canopy interception from satellite observations. *Journal of Geophysical Research-Atmospheres*, 115.
- Mitchell, K. E., Lohmann, D., Houser, P. R., Wood, E. F., Schaake, J. C., Robock, A., Cosgrove, B. A., Sheffield, J., Duan, Q. Y., Luo, L. F., Higgins, R. W., Pinker, R. T., Tarpley, J. D., Lettenmaier, D. P., Marshall, C. H., Entin, J. K., Pan, M., Shi, W., Koren, V., Meng, J., Ramsay, B. H., & Bailey, A. A. (2004). The multi-institution North American Land Data Assimilation System (NLDAS): Utilizing multiple GCIP products and partners in a continental distributed hydrological modeling system. *Journal of Geophysical Research-Atmospheres*, 109.
- Monteith, J. L. (1964). Evaporation and environment. The state of movement of water in living organisms. *Symposium of the society of experimental biology* (pp. 205–234).
- Monteith, J. L. (1973). *Principles of environmental physics*. London: Edward Arnold Press.
- Mu, Q., Heinsch, F. A., Zhao, M., & Running, S. W. (2007). Development of a global evapotranspiration algorithm based on MODIS and global meteorology data. *Remote Sensing of Environment*, 111, 519–536.
- Mueller, B., Seneviratne, S. I., Jimenez, C., Corti, T., Hirschi, M., Balsamo, G., Beljaars, A., Betts, A. K., Ciais, P., Dirmeyer, P., Fisher, J. B., Guo, Z., Jung, M., Kummerow, C. D., Maignan, F., Mccabe, M. F., Reichle, R., Reichstein, M., Rodell, M., Rossow, W. B., Sheffield, J., Teuling, A. J., Wang, K., & Wood, E. F. (2010). Land evapotranspiration: Evaluation of current global observation-based datasets and IPCC AR4 simulations. *Geophysical Research Letters*, In Review.
- Muzylo, A., Llorens, P., Valente, F., Keizer, J. J., Domingo, F., & Gash, J. H. C. (2009). A review of rainfall interception modelling. *Journal of Hydrology*, 370, 191–206.
- Nakai, Y., Sakamoto, T., Terajima, T., & Kitamura, K. (1996). Evaporation of snow intercepted by a todo-fir forest (II). Estimations by an energy balance model and their comparison with water balance measurements. *Journal of Japanese Forest Society*, 78, 15–19.
- Navar, J., & Bryan, R. (1990). Interception loss and rainfall redistribution by 3 semiarid growing shrubs in northeastern Mexico. *Journal of Hydrology*, 115, 51–63.
- Navar, J., & Bryan, R. B. (1994). Fitting the analytical model of rainfall interception of Gash to individual shrubs of semiarid vegetation in northeastern Mexico. *Agricultural and Forest Meteorology*, 68, 133–143.
- Navar, J., Carlyle-Moses, D. E., & Martinez, A. (1999). Interception loss from the Tamaulipan matorral thornscrub of north-eastern Mexico: An application of the Gash analytical interception loss model. *Journal of Arid Environments*, 41, 1–10.
- Navar, J., Charles, F., & Jurado, E. (1999). Spatial variations of interception loss components by Tamaulipan thornscrub in northeastern Mexico. *Forest Ecology and Management*, 124, 231–239.
- Norman, J. M., Anderson, M. C., Kustas, W. P., French, A. N., Mecikalski, J., Torn, R., Diak, G. R., Schmugge, T. J., & Tanner, B. C. W. (2003). Remote sensing of surface energy fluxes at 10(1)-m pixel resolutions. *Water Resources Research*, 39.
- Oren, R., Sperry, J. S., Ewers, B. E., Pataki, D. E., Phillips, N., & Megonigal, J. P. (2001). Sensitivity of mean canopy stomatal conductance to vapor pressure deficit in a flooded *Taxodium distichum* L. forest: hydraulic and non-hydraulic effects. *Oecologia*, 126, 21–29.
- Oren, R., Sperry, J. S., Katul, G. G., Pataki, D. E., Ewers, B. E., Phillips, N., & Schafer, K. V. R. (1999). Survey and synthesis of intra- and interspecific variation in stomatal sensitivity to vapour pressure deficit. *Plant, Cell & Environment*, 22, 1515–1526.
- Ortega-Farias, S., Oliosio, A., Antonioletti, R., & Brisson, N. (2004). Evaluation of the Penman-Monteith model for estimating soybean evapotranspiration. *Irrigation Science*, 23, 1–9.
- Penman, H. L. (1948). Natural evaporation from open water, bare soil and grass. *Proceedings of the Royal Society of London Series a-Mathematical and Physical Sciences*, 193, 120–8.
- Phillips, O. L., Aragao, L. E. O. C., Lewis, S. L., Fisher, J. B., Lloyd, J., Lopez-Gonzalez, G., Malhi, Y., Monteagudo, A., Peacock, J., Quesada, C. A., van der Heijden, G., Almeida, S., Amaral, I., Arroyo, L., Aymard, G., Baker, T. R., Banki, O., Blanc, L., Bonal, D., Brando, P., Chave, J., de Oliveira, A. C. A., Cardozo, N. D., Czimczik, C. I., Feldpausch, T. R., Freitas, M. A., Gloor, E., Higuchi, N., Jimenez, E., Lloyd, G., Meir, P., Mendoza, C., Morel, A., Neill, D. A., Nepstad, D., Patino, S., Penuela, M. C., Prieto, A., Ramirez, F., Schwarz, M., Silva, J., Silveira, M., Thomas, A. S., ter Steege, H., Stropp, J., Vasquez, R., Zelazowski, P., Davila, E. A., Andelman, S., Andrade, A., Chao, K. J., Erwin, T., Di Fiore, A., Honorio, E., Keeling, H., Killeen, T. J., Laurance, W. F., Cruz, A. P., Pitman, N. C. A., Vargas, P. N., Ramirez-Angulo, H., Rudas, A., Salamao, R., Silva, N., Terborgh, J., & Torres-Lezama, A. (2009). Drought sensitivity of the Amazon rainforest. *Science*, 323, 1344–1347.
- Pomeroy, J. W., & Essery, R. L. H. (1999). Turbulent fluxes during blowing snow: Field tests of model sublimation predictions. *Hydrological Processes*, 13, 2963–2975.
- Priestley, C. H. B., & Taylor, R. J. (1972). On the assessment of surface heat flux and evaporation using large-scale parameters. *Monthly Weather Review*, 100, 81–82.
- Reichstein, M., Jung, M., Beer, C., Tomelleri, E., Baldocchi, D., Gobron, N., Rodenbeck, C., & Papale, D. (2009). From point to globe: Up-scaling carbon and water fluxes from FLUXNET EDDY Covariance Tower via integration with Global Earth Observation. *Water in a Changing Climate*. Melbourne, Australia.
- Rodell, M., Houser, P. R., Jambor, U., Gottschalk, J., Mitchell, K., Meng, C. J., Arsenault, K., Cosgrove, B., Radakovich, J., Bosilovich, M., Entin, J. K., Walker, J. P., Lohmann, D., & Toll, D. (2004). The global land data assimilation system. *Bulletin of the American Meteorological Society*, 85, 381–+.
- Roerink, G. J., Su, Z., & Menenti, M. (2000). S-SEBI: A simple remote sensing algorithm to estimate the surface energy balance. *Physics and Chemistry of the Earth. Part B: Hydrology, Oceans and Atmosphere*, 25, 147–157.
- Rossow, W. B., & Duenas, E. N. (2004). The International Satellite Cloud Climatology Project (ISCCP) web site – An online resource for research. *Bulletin of the American Meteorological Society*, 85, 167–172.
- Rudolf, B., Fuchs, T., Schneider, U., Meyer-Christoffer, A., Rudolf, B., Fuchs, T., Schneider, U., & Meyer-Christoffer, A. (2003). *Introduction of the Global Precipitation Climatology Centre (GPCC)* (pp. 16). Deutscher Wetterdienst: Offenbach.
- Rutan, D., Rose, F., Roman, M., Manalo-Smith, N., Schaaf, C., & Charlock, T. (2009). Development and assessment of broadband surface albedo from Clouds and the Earth's Radiant Energy System Clouds and Radiation Swath data product. *Journal of Geophysical Research-Atmospheres*, 114.
- Rutter, A. J. (1967). An analysis of evaporation from a stand of Scots pine. In W. E., & H. W. (Eds.), *Forest hydrology* (pp. 403–417). Oxford: Pergamon.
- Rutter, A. J. (1968). Water consumption by forests. In T. T. (Ed.), *Water deficits and plant growth* (pp. 23–84). Academic Press.
- Rutter, A. J., Kershaw, K. A., Robins, P. C., & Morton, A. J. (1971). A predictive model of rainfall interception in forests. 1. Derivation of the model from observations in a plantation of corsican pine. *Agricultural Meteorology*, 9, 367–384.

- Rutter, A. J., & Morton, A. J. (1977). Predictive model of rainfall interception in forests. 3. Sensitivity of model to stand parameters and meteorological variables. *Journal of Applied Ecology*, 14, 567–588.
- Sandford, A. P., & Jarvis, P. G. (1986). Stomatal responses to humidity in selected conifers. *Tree Physiology*, 2, 89–103.
- Seicz, S., Endrodi, G., & Tajchman, S. (1969). Aerodynamic and surface factors in evaporation. *Water Resources Research*, 5, 380–394.
- Schiffer, R. A., & Rossow, W. B. (1983). The International-Satellite-Cloud-Climatology-Project (ISCCP) – The 1st project of the World-Climate-Research-Programme. *Bulletin of the American Meteorological Society*, 64, 779–784.
- Schulze, E. D., Kelliher, F. M., Korner, C., Lloyd, J., & Leuning, R. (1994). Relationships among maximum stomatal conductance, ecosystem surface conductance, carbon assimilation rate, and plant nitrogen nutrition – A global ecology scaling exercise. *Annual Review of Ecology and Systematics*, 25, (pp. 629–&).
- Sellers, P., Hall, F., Margolis, H., Kelly, B., Baldocchi, D., Denhartog, G., Cihlar, J., Ryan, M. G., Goodison, B., Crill, P., Ranson, K. J., Lettenmaier, D., & Wickland, D. E. (1995). The Boreal Ecosystem-Atmosphere Study (Boreas) – An overview and early results from the 1994 field year. *Bulletin of the American Meteorological Society*, 76, 1549–1577.
- Sellers, P. J., Mintz, Y., Sud, Y. C., & Dalcher, A. (1986). A simple biosphere model (SiB) for use within general-circulation models. *Journal of Atmospheric Sciences*, 43, 505–531.
- Sheffield, J., & Wood, E. F. (2007). Characteristics of global and regional drought, 1950–2000: Analysis of soil moisture data from off-line simulation of the terrestrial hydrologic cycle. *Journal of Geophysical Research-Atmospheres*, 112.
- Shiklomanov, I. A., & Sokolov, A. A. (1985). Methodological basis of world water balance investigation and computation. *New Approaches in Water Balance Computations. Hamburg*.
- Shuttleworth, W. J. (1988). Evaporation from Amazonian rainforest. *Proceedings of the Royal Society of London. Series B: Biological Sciences*, 233, 321–346.
- Shuttleworth, W. J., & Calder, I. R. (1979). Has the Priestley–Taylor equation any relevance to forest evaporation. *Journal of Applied Meteorology*, 18, 639–646.
- Simmons, A. J., Uppala, S. M., Dee, D. P., & Kobayashi, S. (2007). ERA-Interim: New ECMWF reanalysis products from 1989 onwards. *ECMWF Newsletter* (pp. 25–35).
- Stackhouse, P. W., Gupta, S. K., Cox, S. J., Chiacchio, M., & Mikovitz, C. (2000). The WCRP/GEWEX Surface Radiation Budget Project Release 2: An assessment of surface fluxes at 1 degree resolution. *International Radiation Symposium St. Petersburg, Russia*.
- Stannard, D. I. (1993). Comparison of Penman–Monteith, Shuttleworth–Wallace, and modified Priestley–Taylor evapotranspiration models for wildland vegetation in semiarid rangeland. *Water Resources Research*, 29, 1379–1392.
- Su, Z. (2002). The Surface Energy Balance System (SEBS) for estimation of turbulent heat fluxes. *Hydrology and Earth System Sciences*, 6, 85–99.
- Su, H. B., McCabe, M. F., Wood, E. F., Su, Z., & Prueger, J. H. (2005). Modeling evapotranspiration during SMACEX: Comparing two approaches for local- and regional-scale prediction. *Journal of Hydrometeorology*, 6, 910–922.
- Su, Z., Schmutge, T., Kustas, W. P., & Massman, W. J. (2001). An evaluation of two models for estimation of the roughness height for heat transfer between the land surface and the atmosphere. *Journal of Applied Meteorology*, 40, 1933–1951.
- Su, H., Wood, E. F., McCabe, M. F., & Su, Z. (2007). Evaluation of remotely sensed evapotranspiration over the CEOP EOP-1 reference sites. *Journal of the Meteorological Society of Japan*, 85A, 439–459.
- Sugita, M., & Brutsaert, W. (1991). Daily evaporation over a region from lower boundary-layer profiles measured with radiosondes. *Water Resources Research*, 27, 747–752.
- Thorntwaite, C. W. (1948). An approach toward a rational classification of climate. *Geographical Review*, 38, 55–94.
- Twine, T. E., Kustas, W. P., Norman, J. M., Cook, D. R., Houser, P. R., Meyers, T. P., Prueger, J. H., Starks, P. J., & Wesely, M. L. (2000). Correcting eddy-covariance flux underestimates over a grassland. *Agricultural and Forest Meteorology*, 103, 279–300.
- Uppala, S. M., Dee, D. P., Kobayashi, S., Berrisford, P., & Simmons, A. J. (2008). Towards a climate data assimilation system: Status update of ERA-Interim. *ECMWF Newsletter* (pp. 12–18).
- Valente, F., David, J. S., & Gash, J. H. C. (1997). Modelling interception loss for two sparse eucalypt and pine forests in central Portugal using reformulated Rutter and Gash analytical models. *Journal of Hydrology*, 190, 141–162.
- van Dijk, A. I. J. M., & Bruijnzeel, L. A. (2001). Modelling rainfall interception by vegetation of variable density using an adapted analytical model. Part 1. Model description. *Journal of Hydrology*, 247, 230–238.
- Vinukollu, R. K., Sheffield, J., Wood, E. F., Bosilovich, M., & Mocko, D. (2010). Multi-model analysis of energy and water fluxes: Intercomparisons between operational analyses, land surface model and remote sensing. *Journal of Hydrometeorology*. In Review.
- Waggoner, P. E., Begg, J. E., & Turner, N. C. (1969). Evaporation of dew. *Agricultural Meteorology*, 6, 227–&.
- Wan, Z. M., & Li, Z. L. (1997). A physics-based algorithm for retrieving land-surface emissivity and temperature from EOS/MODIS data. *IEEE Transactions on Geoscience and Remote Sensing*, 35, 980–996.
- Wan, Z., Wang, P., & Li, X. (2004). Using MODIS land surface temperature and normalized difference vegetation index products for monitoring drought in the southern Great Plains, USA. *International Journal of Remote Sensing*, 25, 61–72.
- Wan, Z., Zhang, Y., Zhang, Q., & Li, Z. L. (2004). Quality assessment and validation of the MODIS global land surface temperature. *International Journal of Remote Sensing*, 25, 261–274.
- Wang, K. C., Li, Z. Q., & Cribb, M. (2006). Estimation of evaporative fraction from a combination of day and night land surface temperatures and NDVI: A new method to determine the Priestley–Taylor parameter. *Remote Sensing of Environment*, 102, 293–305.
- Wilm, H. G. (1944). Report of the committee on transpiration and evaporation, 1943–44. *Transactions of the American Geophysical Union*, 25, 683–693.
- Wright, I. R., Manzi, A. O., & Darocha, H. R. (1995). Surface conductance of Amazonian pasture – Model application and calibration for canopy climate. *Agricultural and Forest Meteorology*, 75, 51–70.
- Xu, L. K., & Baldocchi, D. D. (2003). Seasonal trends in photosynthetic parameters and stomatal conductance of blue oak (*Quercus douglasii*) under prolonged summer drought and high temperature. *Tree Physiology*, 23, 865–877.
- Zeng, X. B., Dickinson, R. E., Walker, A., Shaikh, M., DeFries, R. S., & Qi, J. G. (2000). Derivation and evaluation of global 1-km fractional vegetation cover data for land modeling. *Journal of Applied Meteorology*, 39, 826–839.
- Zinke, P. J. (1967). Forest interception studies in the United States. In W. E. Sopper & H.W. Lull (Eds.), *Forest hydrology* (pp. 137–161). Oxford: Pergamon.